



1 **Assessment of potential seismic hazard for sensitive facilities** 2 **by applying seismo-tectonic criteria: an example from the** 3 **Levant region**

4 Matty Sharon^{1,2}, Amir Sagy¹, Ittai Kurzon¹, Shmuel Marco², Marcelo Rosensaft¹

5 1. Geological Survey of Israel, Jerusalem 9371234, Israel

6 2. Porter School of the Environment and Earth Sciences, Tel Aviv University, Tel Aviv
 7 6997801, Israel

8 *Correspondence to:* Amir Sagy (asagy@gsi.gov.il)

9

10

11 **Abstract**

12 We present a methodology for mapping faults that constitute a potential hazard to
 13 structures, with an emphasis on special facilities such as dams and nuclear power plants.
 14 The methodology categorises faults by hierarchical seismo-tectonic criteria, which are
 15 designed according to the degree of certainty for recent activity and the accessibility of
 16 the information within a given region. First, the instrumental seismicity is statistically
 17 processed to obtain the gridded seismicity of the earthquake density and the seismic
 18 moment density parameters. Their spatial distribution reveals the zones of the seismic
 19 sources, within the examined period. We combine these results with geodetic slip rates,
 20 historical earthquake data, geological maps and other sources to define and categorise
 21 faults that are likely to generate significant earthquakes ($M \geq 6.0$). Their mapping is
 22 fundamental for seismo-tectonic modelling and for PSHA analyses. In addition, for
 23 surface rupture hazard, we create a database and a map of capable faults, by developing
 24 criteria according to the regional stratigraphy and the seismotectonic configuration. The
 25 relationship between seismicity slip dynamics and fault activity through time is an
 26 intrinsic result of our analysis that allows revealing the tectonic evolution of a given
 27 region. The presented methodology expands the ability to differentiate between
 28 subgroups for planning or maintenance of different constructions or for research aims,
 29 and can be applied in other regions.



30 1. Introduction

31 The establishment of sensitive facilities such as nuclear power plants or dams have
32 been raising the seismic risk to higher levels and entail the need for a profound
33 understanding of the seismic hazard (e.g. Marano et al., 2010). Probably the most famous
34 example is the destruction of the Fukushima nuclear power plant by tsunami waves
35 caused by the 2011 $M_w = 9.0$ Tohoku-oki earthquake, which has been affecting an
36 extensive region ever since. Identifying and characterising the regional seismic sources
37 and their potential hazard is therefore fundamental for siting and designing of potential
38 facilities, and for risk management. Additionally, in the case of infrastructures, the hazard
39 also includes surface rupture in close proximity to the construction. The goals of this
40 study are to define the regional main seismic sources, presuming that these are the
41 sources that are likely to generate the most significant earthquakes in the near future, and
42 to minimise the likelihood of surface rupture at the underlying infrastructure of sensitive
43 facilities.

44 Despite the limited duration of the instrumental record, it constitutes one of the main
45 direct evidence of fault activity in the current tectonic configuration. Probabilistic
46 analyses of seismicity can constrain fault locations, kinematics and activity rates (e.g.
47 Woo, 1996; Atkinson and Goda, 2011). Moreover, the Gutenberg-Richter empirical law
48 allows assessing the frequency of medium to strong earthquakes by extrapolating low-
49 magnitude earthquakes. Since surface ruptures are usually associated with $M \geq \sim 6.0$
50 (Wells and Coppersmith, 1994; Stirling et al., 2002), the concentration of seismicity
51 along faults highly suggests that surface ruptures occurred in the recent geological
52 history. However, due to the scarcity of large earthquakes in the instrumental era,
53 complementary information is required for further constraining the location of the main
54 sources of significant earthquakes, and for characterising them. . This information can
55 come from archaeological and paleo-seismological investigations, and from historical
56 documents (e.g. Ambraseys, 2009; Agnon, 2014; Marco and Klinger, 2014). Geodetic
57 measurements of relative displacements and velocities provide further crucial kinematic
58 information (Baer et al., 1999; Hamiel et al., 2016; 2018a; 2018b).



Detailed geological investigation of faults can further extend the necessary information, in particular for long-term activity. In terms of seismic hazard perspective, faults that were active in the recent geological periods have a larger probability for future faulting, compared with other faults. Field relations between faults and geological units, as revealed in geological maps, can force constraints on the location, timing and the amount of offset of the relevant faults. However, these evidences are limited to places where faults have field relationships with young formations. Since the spatial distribution of such formations can be limited, additional criteria are required for mapping potentially hazardous faults.

In this paper we incorporate independent datasets to produce a variety of essential products for seismic hazard evaluation, including surface rupture and ground motion. We demonstrate it for the Israel region, a seismically-active zone mainly affected by the Dead Sea Transform fault system (DST; Fig. 1). We first determine the main seismic sources in Israel and its vicinity, focusing on faults that are likely to generate intermediate to large earthquakes. Subsequently, we present the process utilised to determine and map faults that constitute a potential hazard of surface rupture for sensitive facilities. We design the criteria according to the likelihood of surface rupture along specific faults.

76

77 2. Tectonic settings

The continental crust in the region of Israel was formed during the Pan-African orogeny of Late Precambrian age, and was later subjected to alternating periods of sedimentation and erosion during the Paleozoic (Garfunkel, 1998). Continental breakup and the establishment of passive margins along the Tethys-Mediterranean coast of the Levant occurred during the Triassic-Jurassic time. Widespread carbonate platform developed during the mid-Cretaceous. Since the Upper Cretaceous, the region was subjected to WNW compression of the Syrian-Arc system, deforming the sedimentary sequence into a series of asymmetric folds, strike-slip faults, and monoclines (Eyal and Reches, 1983; Sagy et al, 2003). Regional uplift began from the end of the Eocene and the area was intermittently exposed to erosional processes (Picard, 1965). The African-Arabian plate broke along the suture of Gulf-of-Aden, Red Sea during the Miocene,



89 generating the Suez rift and the DST which separate the Sinai sub-plate from the African
 90 and the Arab plates (Fig. 1). The Suez rift, however, has shown relatively minor signs of
 91 deformation since the end of the Miocene (Garfunkel and Bartov, 1977; Joffe and
 92 Garfunkel, 1987; Steckler et al., 1988), while the DST system remains the most active
 93 tectonic feature in the area. In the Easternmost Mediterranean, the current plate boundary
 94 deformation is taking place along the convergent Cyprian Arc (Fig. 1), where the
 95 Anatolian plate overrides the plates of Africa and Sinai (e.g., McKenzie, 1970).

96 The 1000-km DST is the largest fault system in the east-Mediterranean region (Fig.
 97 1). Its northern section crosses northwest Syria in a N-S orientation; several recent large
 98 earthquakes were attributed to this section during the past two millennia (Meghraoui et
 99 al., 2003). The middle section of the DST is a restraining bend (LRB; Fig. 1),
 100 characterised by transpression deformation (Quennell, 1959). The section is branched to a
 101 few segments that transfer the main component of the strike-slip motion in Lebanon area
 102 (Gomez et al., 2003; 2007). The Israel region is located along the southern section of the
 103 DST but seismically it is also affected by the activity of the middle part.

104 The southern part of the DST (Fig. 1) is dominated by a sinistral motion of
 105 approximately ~5 mm/yr, summing up to ~105-km of left-lateral displacement over a
 106 period of 15-20 million years (e.g. Garfunkel, 1981; 2014). It is marked by a pronounced
 107 5–25 km wide topographic valley, mostly with uplifted flanks, bordered by normal faults
 108 that extend along the valley margins. The lateral motion occurs on longitudinal left-
 109 stepping strike-slip and oblique-slip fault segments. The strike slip segments delimit a
 110 string of en-echelon arranged rhomb-shaped narrow and deep releasing bends that are
 111 associated with orthogonal separation of the transform flanks on the surface, which may
 112 well extend beneath the crust (Garfunkel, 1981; Garfunkel and Ben-Avraham, 2001;
 113 Wetzler et al., 2014). The seismic potential was clearly expressed by the 1995 $M_w = 7.2$
 114 Nuweiba earthquake in the Gulf of Elat (Aqaba), the largest seismic event documented
 115 instrumentally on the DST. Historical and prehistorical large earthquakes are also well
 116 documented (e.g. Marco, 2008; Marco et al., 2005; Amit et al., 2002). The slip rates
 117 along the DST vary between different fault segments and time resolutions, but converges
 118 at about 4–5 mm/yr, approximately the same values obtained by GPS measurements
 119 (Marco and Klinger, 2014; Hamiel et al., 2018a; 2018b). Deep-crust seismicity is



120 significant along the southern part of the DST in correlation with areas of low heat flow,
 121 particularly along the Dead Sea Basin, probably indicating a cool and brittle lower crust
 122 (Aldersons et al., 2003; Shalev et al., 2007; 2013).

123 The Sinai sub-plate south to Lebanon displays some amount of internal deformation
 124 expressed by a few fault systems, which are associated with Quaternary activity. The
 125 Carmel-Tirza Fault zone (CTF; Fig. 1) consists of a few normal and oblique fault
 126 segments generally striking NW-SE. The system is characterised by low heat flow and by
 127 relatively deep seismicity (Hofstetter et al., 1996; Shalev et al., 2013). The CTF divides
 128 the Israel-Sinai sub-plate into two tectonic domains (Neev et al., 1976; Sadeh et al., 2012)
 129 where the southern part is assumed to be relatively rigid, while northward, normal faults
 130 orientated E-W generate N-S extension expressed by graben and horst structures (Ron
 131 and Eyal, 1985).

132

133 3. Geological Database

134 The database of faults that were active in the recent geological history is mainly based
 135 on high-resolution geological maps. As of January 2019, 71 geological map sheets in the
 136 scale of 1:50,000 are available for this study, out of the 79 sheets required to cover the
 137 whole state of Israel (Fig. A1). The 1:200,000 geological map of Israel (Sneh et al., 1998)
 138 is utilised where 1:50,000 data are absent. Included also are faults defined as active or
 139 potentially active for the Israel Standard 413 "Design provisions for earthquake resistance
 140 of structures" (Sagy et al., 2013). In addition, some faults that have not been mapped (or
 141 not updated yet) crossing Quaternary units in the geological maps, are marked here as
 142 Quaternary faults based on evidence presented in scientific publications, reports, and
 143 theses (see Table A1).

144 The establishment of Quaternary formation database (Table A2), to constrain fault
 145 activity in this study is complicated due to poorly constrained geochronology of some of
 146 the formations. In some cases the age uncertainty is in the order of millions of years.
 147 Moreover, the boundary Pleistocene-Pliocene (Neogene-Quaternary) was shifted in 2009,
 148 from ~1.8Ma to ~2.6Ma. Thus, some formations that had previously been assigned
 149 Pliocene age became part of the Pleistocene. Therefore, geological periods attributed to



150 some formations, mentioned in pre-2009 publications, might mislead. Many stratigraphic
151 charts of the pre-2009 geological maps are outdated. Furthermore, as recent research
152 provides better geochronological constraints, the most up-to-date information is required
153 in order to correctly select Quaternary formations. In Appendix 1 (Table A1) we present
154 references to Quaternary faults that cannot be directly deduced from the geological maps.

155 Beside the surface traces of mapped faults, offshore and subsurface continuation of
156 faults, as well as faults extending beyond the Israeli borders were added to the database
157 (Table A3). The latter are limited to the extensions of mapped faults that are within
158 Israel, and/or the main DST segments. The criteria for selecting these faults are discussed
159 in section 6.

160

161 4. Seismological analysis

162 We analyse the spatial distribution of seismic events in order to reveal the regional
163 seismic pattern, which helps to define the main seismic sources and develop an
164 independent criterion for Quaternary active faults. In order to define the seismicity-based
165 criterion, we design seismic criteria that are based on the distribution of two parameters:
166 the *Earthquake Kernel Density* and the *Seismic Moment Kernel Density*. We demonstrate
167 the methodology and then present the results below.

168

169 4.1 Dataset

170 We use an earthquake catalogue from 1.1.1983 until 31.8.2017 within 28°N – 34°N
171 and 33°E – 37°E, recorded by ~140 stations whose distribution has changed in time and
172 space. Most of the data are from the Israel Seismic Network (ISN), the Comprehensive
173 Nuclear Test-Ban Treaty (CTBT), and the Cooperating National Facility (CNF). Some
174 additional data were incorporated from other regional networks: GE, GEOFON global
175 network of Deutsches GeoForschungsZentrum, Potsdam (GFZ), Jordanian Seismic
176 Observatory (JSO), and the seismic network of Cyprus (CQ). These earthquakes, which
177 have been monitored by the Seismological Division of the Geophysical Institute of Israel,
178 comprise a catalogue of ~17,600 earthquakes. They were relocated (Fig. 2) to generate a



179 new catalogue with more precise locations of hypocentres (Wetzler and Kurzon 2016).
 180 As part of the relocation process, ~900 earthquakes were excluded for various reasons,
 181 e.g., events that were recorded by less than 4 stations; large location errors (including the
 182 $M_d = 5.8$ 1993 event in the Gulf of Elat). Before 1983 the locations are less reliable.
 183 Hence, the relocated catalogue consists of ~16,700 events of $0.1 \leq M \leq 7.2$ (Fig. 2).
 184 Earthquakes with unknown magnitudes received a default value of $M = 0.1$. The
 185 magnitude and the location of the $M_w = 7.2$ 1995 Nuweiba earthquake were fixed
 186 according to Hofstetter et al. (2003).

187 In order to assess the applicability of the following seismic processing and analysis,
 188 we define the network coverage area as the zone in which the hypocentres are relatively
 189 well-constrained. This is examined and determined here as the polygon that covers all
 190 seismic stations that recorded at least 350 arrivals, and consists of the smallest number of
 191 polygon-sides that link between the stations (Fig. A2 in Appendix 2).

192

193 **4.2 Spatial data processing**

194 In order to quantitatively characterise the regional seismicity and associate the
 195 earthquakes with mapped faults we examine two parameters: a) *earthquake kernel*
 196 *density* and b) *seismic moment (M_0) kernel density*. Both parameters are obtained through
 197 the following spatial data processing. A regional scan is carried out in a 0.5-km interval
 198 2D grid, in the horizontal coordinates. For each grid point, both parameters are calculated
 199 for the events within a 6-km distance of the grid point. The parameters are calculated
 200 based on the kernel density estimation as an approach to obtain the spatial distribution
 201 through a probability density function, using the distance to weight each event from a
 202 reference point (each grid point). The weighting can be illustrated as many circles of up
 203 to 6-km radius that surround a common centre (every grid point). The circle shape
 204 prevents any directional bias.

205 The 6-km radius from each grid-point, and the Gaussian function and its standard
 206 deviation of 2 (for the kernel estimation), were tuned and chosen to: a) capture different
 207 seismic patches along active faults; b) be significantly larger than the location horizontal
 208 median error (~1.2 km; Wetzler and Kurzon, 2016); c) assign higher weight to events



209 closer to the evaluated grid-point; d) include as many events as possible for achieving
 210 statistical significance at each of the grid-points.

211 The *earthquake kernel density* parameter, ρ_{Nk} , is calculated by counting all the
 212 weighted events within a 6-km radius from each grid point, dividing their sum by the
 213 sampler area (πr^2) and normalising by the duration of the earthquake catalogue:

$$214 \quad \rho_{Nk} = \frac{\sum_{n=1}^N e^{-\frac{d(n)^2}{2\sigma^2}}}{T\pi r^2} \quad (1)$$

215 where N is the total number of events within the radius r , $d(n)$ is the distance between an
 216 event n and the circle centre; σ is the standard deviation of the Gaussian function, and T
 217 is the duration of the earthquake catalogue. Units are [*events/km²/yr*].

218 The M_0 *kernel density* parameter, ρ_{M0k} , is obtained by first calculating the seismic
 219 moment released by each event separately, using the empirical relation between M_0 and
 220 M_L , as obtained by Shapira and Hofstetter (1993) after converting units from *dyne-cm* to
 221 *N-m*:

$$222 \quad \log[M_0] = 10 + 1.3M_L \quad (2)$$

223 Secondly, each amount of energy is weighted according to the distance of the
 224 corresponding event from the circle centre (like the calculation of the *earthquake kernel*
 225 *density*). Then, we sum the weighted- M_0 released from all the events within a 6-km
 226 radius, divide the sum by the circle area (πr^2) and normalise by the duration of the
 227 catalogue:

$$228 \quad \rho_{M0k} = \frac{\sum_{n=1}^N M_0(n) e^{-\frac{d(n)^2}{2\sigma^2}}}{T\pi r^2} \quad (3)$$

229 where N is the total number of events within the radius r , $M_0(n)$ is the seismic moment
 230 released from an event n according to Eq. 2, $d(n)$ is the distance between an event n and
 231 the circle centre, σ is the standard deviation of the Gaussian function, and T is the
 232 duration of the earthquake catalogue; units are [*joule/km²/yr*].

233

234



235 **4.3 Distribution maps of the spatial processing parameters**

236 *4.3.1. Earthquake Kernel Density*

237 The *earthquake kernel density* (Fig. 3) captures the main active tectonic sources and
 238 seismic patches, according to ~35 years of instrumental seismicity. As expected, most of
 239 the earthquakes are concentrated along the main fault zone of the DST, and to a lesser
 240 extent along the CTF, including its offshore continuation in the Mediterranean Sea. In the
 241 southwest, seismicity is observed in the area of the Gulf of Suez. Small patches appear in
 242 different spots, mainly west of the DST, raising the issue of the detectability of the
 243 network east of it. We note that the International Seismological Centre catalogue reveals
 244 large portion of events recorded east of the DST as well (Palano et al., 2013). The most
 245 prominent zone of seismicity that is not associated with known active tectonic feature is
 246 northwest of the Gulf of Elat.

247 A more detailed scan of the seismicity from south shows that the prominent patches
 248 of seismicity along the DST are located in the Gulf of Elat, the Arava valley, and the
 249 Dead Sea Basin. Northwards, seismicity becomes more distributed, reflecting the
 250 intersection between the DST and the CTF (Fig. 1). North of the intersection, the Jordan
 251 valley segment of the DST is sparse with seismicity. However, further north, dominant
 252 seismicity patches are seen in the Sea of Galilee, and in the Hula valley. Northwest of the
 253 Hula valley, another zone of intense seismicity is captured, which might be associated
 254 with faults related to the Roum fault, west of the LBR (Meirova and Hofstetter, 2013).

255

256 *4.3.2. Seismic moment kernel density*

257 The distribution of the average annual moment density released from all earthquakes,
 258 assuming them as point sources, is shown in figure 4. Since the amount of energy
 259 released by each earthquake differs significantly according to its magnitude, this
 260 parameter is presented on a logarithmic scale. Overall, the *Mo kernel density* distribution
 261 emphasises the seismic activity along the DST, with similarity to the *earthquake kernel*
 262 *density* distribution (Fig. 3). Still, the distribution is less smooth due to single events
 263 differing significantly from each other in their corresponding Mo release.



264 The Gulf of Elat includes the largest event recorded in the catalogue, the $M_w = 7.2$
 265 1995 Nuweiba earthquake (Hofstetter et al., 2003), two order of magnitudes larger than
 266 the second-largest event ($M_d = 5.6$), hence the significantly higher values in its vicinity.
 267 The spatial distribution of the *Mo kernel density* reveals a wide zone of deformation
 268 surrounding the gulf flanks, much wider than the relatively narrow gulf. This can be
 269 partially explained by the poorly-constrained epicentre locations, far away from the
 270 network coverage (Fig. A2). The *seismic moment kernel density* reflects strongly the most
 271 significant events that occurred in the past 35 years; among them are the $M_w = 5.1$ 2004
 272 event in the Dead Sea (Hofstetter et al., 2008), and the $M_d = 5.3$ 1984 event associated
 273 with the CTF. In contrast with the distribution of the *earthquake kernel density*, the *Mo*
 274 *kernel density* does not reflect seismic swarms, unless they consist of high magnitudes.
 275 This contrast is predominant in the Sea of Galilee, which contains high *earthquake kernel*
 276 *density* (Fig. 3) but is less significant in the *seismic moment kernel density* (Fig. 4).

277

278 5. The main seismic sources

279 Figures 3 and 4 show a strip of dense seismic events and moment release along the
 280 DST and its main branches. We now combine these data with geologic, geodetic and
 281 paleoseismologic measurements to generate the main seismic sources map, which
 282 displays regional faults that demonstrates slip rates inferred here as $\geq 0.5\text{mm/yr}$ during
 283 the Holocene. Tectonic and geometric characteristics (i.e., segment length & orientation)
 284 are also considered. We define the main seismic sources as faults that are likely to
 285 generate significant earthquakes ($M \geq 6.0$), which can impact Israel and constitute
 286 potential sources for different sorts of damages (i.e., ground motion and acceleration,
 287 landslides, liquefactions and tsunamis). These faults and their map (Fig. 5) are essential
 288 for seismotectonic modelling of Israel, Probabilistic Seismic Hazard Analysis (PSHA)
 289 and eventually for generating ground motion maps. Below, we define two subgroups of
 290 faults divided by their tectonic characteristics and their slip rates. Off-shore inferred
 291 continuations of the main faults are also presented (dashed lines in Fig. 5).

292 5.1 Potential sources for large earthquakes



293 This category (solid black lines in Fig. 5) includes the main sinistral and oblique fault
 294 segments of the DST in the region. According to paleoseismic and/or geodetic
 295 investigations (Table 5), these faults are associated with Holocene slip rates of $1 \text{ mm/yr} <$
 296 $V_S < 5 \text{ mm/yr}$, where V_S is the average sinistral slip component accommodated by these
 297 faults. Equally important, all the faults in this category are relatively long with a
 298 preferable slip orientation according to the present stress field (Jaeger et al., 2007). Our
 299 database (Fig. 5) includes fault segments from this subgroup which are located up to 150-
 300 km away from Israel. As noted in Sec. 4, the only recorded large earthquake, the 7.2 M_w
 301 Nuweiba earthquake occurred on the Aragonese Fault and was associated with mean slip
 302 of 1.4–3 m (Baer et al., 1999).

303 South to Lebanon, geodetic measurements show $\sim 4\text{--}5 \text{ mm/yr}$ sinistral slip (Hamiel et
 304 al., 2016; 2018a; 2018b; Masson, 2015). Faulting in Lebanon is partitioned to a few
 305 branches (Fig. 3) and the specific rates are less constrained. While the Yammuneh and
 306 the Serghaya faults can undoubtedly be considered as independent sources for significant
 307 earthquakes, the status of the shorter, Rachaiya and Roum fault branches are less clear.
 308 Nevertheless, according to the present state of information (see for example, Nemer and
 309 Meghraoui (2006)), we cannot rule them out and they remain part of this group.

310 Previous analyses of maximum earthquake magnitude based on historical earthquakes
 311 or on background seismicity predicted magnitudes of $\leq 7.8 M_w$ for the largest segments
 312 (e.g., Stevens and Avouac., 2017; Klinger et al., 2015; Hamiel et al., 2018a).



314 5.2. Potential sources for intermediate earthquakes

315 This category (pale blue lines in Fig. 5) consists of fault zones with lengths of several
 316 dozen kilometres that are associated with the DST, and display estimated slip rates of 0.5
 317 $\text{mm/yr} \leq V_S \leq 1 \text{ mm/yr}$ (Table 6).

318 This subgroup includes the fault zone in the western and eastern margins of the Dead
 319 Sea; the marginal faults of the Hula basin and the CTF (Fig. 5). The partitioning of the
 320 slip rate across parallel segments in any given fault zone is usually below the geodetic



321 measurement (or the information) resolution. Therefore, the segments of this category in
 322 Figure 5 are representative, but not necessarily the most active within a given system.

323

324 Due to the lack of reliable historical and paleo-seismological evidences, the
 325 evaluation of maximum possible magnitude on these faults is usually hard and requires
 326 several assumptions. First, we consider here local rupture on a segment from a given
 327 system and disregard a rupture of the entire system as part of an extremely large
 328 earthquake on the main strike-slip faults (such a rupture is discussed in Sec. 5.1). In
 329 addition, we assume that the longest possible subsurface rupture length is similar to the
 330 length of the segment's surface trace. For example, the Carmel Fault, the northern fault in
 331 the CTF is up to 40-km length (on and off shore). According to some published scaling
 332 relationships, rupturing along its entire length can be associated with up to $\sim 7 M_w$
 333 earthquakes (Wells and Coppersmith, 1994; Stirling et al., 2013). However, we assume
 334 again that such magnitudes must be interconnected with an earthquake along a much
 335 larger DST segment, and not confined to a local fault (Agnon, 2014). We therefore
 336 assume a maximum rupture length of $\sim 10\text{--}20$ km along faults from this subgroup and
 337 correspondingly to maximum magnitudes of $6.0 < M_w < 6.5$ (Wells and Coppersmith,
 338 1994). The data on the Elat Fault is based only on evidence from its northern edge while
 339 the rates at its offshore parts are less constrained. Shaked et al. (2004) inferred a
 340 catastrophic event at 2.3ka on the Elat Fault.

341 Large earthquakes along the Cyprian Arc (Fig. 1) can also generate tsunamis that
 342 might affect the coastline of Israel (Salamon et al., 2000). This source is not analysed and
 343 mapped here, but should be taken into account in regional seismotectonic models.

344

345 6. Capable faults

346 6.1 Framework and principles

347 The hazard of surface rupture is defined as the likelihood of an earthquake that will
 348 rupture the surface within a certain time window. This likelihood is based on knowledge
 349 about the past and present fault kinematics and dynamics. The determination of the
 350 relevant time reference for young faulting is usually dictated by different constraints and



351 applications. In the United States, faults are commonly considered to be active for
352 planning constructions if they have ruptured the surface at least once in the past 10ka.
353 However, regional conditions, such as sedimentary cover or available age dating of
354 pertinent geological units can affect this determination. For example, faults that are
355 defined as “Active” in the “Design Provisions for Earthquake Resistance of Structures” in
356 Israel are those that ruptured the surface in the past 13ka (Heimann, 2002). This is the age
357 of the top of the lake formation that covers significant parts of the Dead Sea valleys.

358 The time reference for special constructions such as dams and nuclear power plants is
359 usually much longer, because the possible damage to the construction has severe regional
360 implications. According to the International Atomic Energy Agency (IAEA) Safety
361 Fundamentals (2010), capable faults are these with evidence for displacement since
362 thousands or millions of years, depending on the region activity. Here, the Quaternary
363 period is selected as the time reference for sensitive facilities due to two main reasons: a)
364 we assume that faults that were active during the present regional stress regime (Zoback,
365 1992) are more likely to activate in the near future. The regional stress state within the
366 Quaternary period is represents well the current stress field (Eyal and Reches, 1983;
367 Hofstetter et al., 2007; Garfunkel, 2011; Palano et al., 2013). We note that “regional
368 stress field” (Zoback, 1992) as a criterion for active faulting is closely related to the
369 “tectonic regime” suggested by Galadini (2012). b) Quaternary geological units are
370 mostly well defined in the region.

371 The primary and secondary criteria for sorting the faults are listed in a descending
372 order of categorisation, meaning that faults are initially examined according to the first
373 criterion, and only if they do not match it, they are examined according to the second
374 criterion, and so on.

375 Finally, in regions where Quaternary cover is absent, we utilise a seismological
376 criterion (Fig. 6), based on the assumption faults that are associated with seismically
377 active subzones are more likely to have ruptured the surface in the Quaternary compared
378 to others.

379

380



381 6.2 Primary criteria

- 382 1. Main strike-slip faults of the DST: identified here as main sources for large regional
 383 earthquakes (Fig. 7).
- 384 2. Faults with direct evidence of Quaternary activity: faults that have been mapped
 385 offsetting Quaternary formations or that have been interpreted by scientific
 386 publications (Table A2) to rupture the earth's surface at least once since the
 387 Quaternary. This criterion is mainly related to zones covered by Quaternary units.

388

389 6.3 Secondary criteria

390 Faults that have no field relationship with Quaternary formations consequently show no
 391 direct evidence for Quaternary faulting. We therefore designed the next criteria under the
 392 rationale that they expand the database with faults that reasonably have been active since
 393 the Quaternary, based on the following three sub-criteria:

- 394 1. First order branches and the marginal faults of the DST
 - 395 a) First order branches of faults that are mapped following the primary criteria. A
 396 fault branch is defined here as splitting at an acute angle from another fault. The
 397 throw direction of the fault and its branches are also taken into account.
 - 398 b) Faults that bound the DST basins, separating Quaternary formations from older
 399 rocks and are associated with a sharp topographic boundary of at least 100 meters.
 - 400 c) Faults that emerge from Quaternary sediments that infill the DST valleys and are
 401 likely to branch off of the main DST segments.

402 2. Faults associated with recent seismicity

403 it is challenging to match the faults and recent seismicity and assume they ruptured
 404 the surface at least once since the beginning of the Quaternary because there are
 405 thousands of mapped faults, high-resolution geophysical data about the fault
 406 structures in depth are scarce, and the hypocentres' location uncertainties are large.
 407 In order to define the seismicity-based criterion, we create polygons for each of the
 408 parameters. The polygons are defined by a threshold value, so that each of them is



the smallest to cover the most active tectonic in the region, continuously in this case, the DST; excluding the relatively silent northern section of the Jordan Valley segment (I in Fig. 6). Therefore, the overlap area (Fig. 6) of the two polygons consists of at least the minimum level of both *seismic moment kernel density* and *earthquake kernel density*, along the DST in the Israel region. Hence, if a fault is within the overlap area, it means that it is associated with at least a minimum level of seismicity along the most active tectonic feature, and thus it is likely to be seismogenic. We further assume a relation between a fault mapped surface trace and a possible past surface rupture, in order to select the most prominent faults. Considering scaling relations between fault dimensions and source parameters, faults that contain surface traces of at least 6-km (corresponding to $M_w \geq 6.0$ earthquakes; Wells and Coppersmith, 1994; Stirling et al., 2002; Mai and Beroza, 2000) within the ‘overlap area’ are assumed here as Quaternary faults.

3. Subsurface faults

Subsurface and offshore continuation of the main DST strike-slip segments, and a few other faults with published details for both their subsurface extension and their Quaternary activity are marked (the majority are in Fig. 5). In addition, we map other faults that offset dated Quaternary units, with well-constrained near-surface location inferred from high-resolution seismic data. We exclude subsurface faults when their exact location and activity period less constrained. Fault segments that were mapped as concealed (mostly by thin alluvium) in the 1:50,000 maps and are the continuation of Quaternary faults are marked as ordinary surface traces.

431

7. Discussion

Regions with intermediate seismicity rates present a challenge for hazard evaluation; while the hazard is perceptible, the seismic data is sparse comparing to very active zones. Taking into the account that the earthquake phenomenon is a stochastic process and its predictability is limited, we develop a methodology that takes advantage of incorporating interdisciplinary information with statistical analyses for seismic hazard evaluation. We delineate the distribution of the density of earthquakes and of the seismic moment release



439 by analysing recorded seismicity and applying statistic-based data processing (Figs. 3, 4).
440 However, instrumental seismological data is practically limited, and the precision of the
441 results depends on the amount and the quality of the data, regardless of the specific
442 statistical method. This gap is closed by geodetic measurements, paleo-seismology and
443 historical information.

444 Throughout the capable fault map (Fig. 7), the information about the seismic intervals
445 of most of the faults is poor compared with these of the DST main strike-slip faults.
446 Faults of different categories are distributed in the same areas: these that show direct
447 evidence of Quaternary faulting, and those that fit seismo-tectonic criteria. For example,
448 branches of the DST main segments that do not cross Quaternary sediments, are marked
449 based on tectonic rationale. Moreover, although faults are marked by hierarchical criteria,
450 in many cases the different categories complement each other rather than show hierarchy
451 of the activity level. Accordingly, the distribution of the different faults is rather
452 homogeneous throughout the map (Fig. 7). This includes faults marked based on the
453 seismicity-based criterion. The Quaternary faults are superimposed on the seismicity
454 polygons of this criterion (Fig. A3) and reveal that many the majority of the faults, which
455 are mapped based on the geological criteria, could have enter the map also by the
456 seismological criterion (ignoring its 6-km fault length limitation). Thus, the correlation
457 between the recorded seismicity and the Quaternary faults support the design of the
458 seismicity-based criterion. On the other hand, we do not define faults that constitute a
459 mechanical potential for slip (for example, conjugate fault sets) as capable, unless further
460 geological or seismological evidence for Quaternary activity is existed. Such a
461 mechanical criterion, however, should be considered and re-evaluated during the specific
462 siting stage.

463 While most of the seismic activity follows the DST, some areas along it are associated
464 with very sparse seismicity (Fig. 6). At the northern section of the Jordan Valley
465 segment, section I is the least active part of the DST during the last ~35 years. Geodetic
466 analysis demonstrates that this section creeps at a rate of approximately half of the total
467 plate motion (Hamiel et al., 2016). This creep, together with potential partitioning of the
468 activity to the CTF, might cause the relative reduction of earthquakes in section I (Fig. 6).
469 Sections II and III, at the middle and the northern sections of the Arava segment, are also



470 associated with sparse seismicity, but to a lesser extent. With no indication for creep, the
471 reduction of seismicity might be attributed to local locking of the main fault or to the
472 influence of other structures in fault junctions (e.g. WSW-ENE orientated faults of the
473 Sinai-Negev shear belt (Bartov, 1974)). Further research of these zones is required for
474 better understanding the local variation of the seismic patterns.

475

476 8. Conclusions

477 1. Mapping and characterising faults that pose seismic hazard require generating
478 interdisciplinary regional database and developing hierarchical seismo-tectonic criteria.

479 With respect to the specific dictated requirements, faults that are potential sources for the
480 far-field and for the near-field (i.e., surface rupture) hazards should be analysed by
481 different criteria; both represent seismic hazard of significant earthquakes but within
482 different time frames.

483 2. The regional main seismic sources are primarily defined by the recent slip rates.
484 Geologic and geodetic slip rates, as well as long historical record and high-resolution
485 mapping enable reliable definition of faults that are likely to generate large earthquakes.
486 All the main seismic sources in the Israel region (Fig. 5) are related to the DST activity.

487 3. The time reference for local planning of special constructions such as dams and
488 nuclear power plants is usually long, because the possible damage to the construction has
489 severe regional implications. We selected the Quaternary period as the relevant time
490 frame for capable faults in the region of Israel. While this time frame (2.6 Ma) is longer
491 than the previous for defining capable faults for a potential local nuclear power plant
492 (IEC and WLA, 2002), it is justified by considering the regional stress field, the regional
493 stratigraphic configurations and the criteria that focus on surface rupture rather than
494 general fault movements. We conclude that tectonic and stratigraphic conditions, as well
495 as the accessibility of geologic maps and their resolutions, should be taken into account
496 for defining the time frame for capable faults.

497 4. We design a seismicity-based criterion that is based on the distribution of two
498 parameters: the *Earthquake Kernel Density* and the *Seismic Moment Kernel Density*. The



499 success of this selection is further reinforced by the match between the geological-
 500 categorised faults and the seismicity criterion (Fig. A3).

501 5. Beyond planning of special constructions, the developed database and the maps
 502 that are generated and presented here constitute further applications for planning and
 503 research. The regional main seismic sources map (Fig. 5) is fundamental for
 504 seismotectonic modelling and eventually for generating ground motion prediction maps
 505 (e.g. by PSHA) that include essential information for construction planning, such as peak
 506 ground acceleration. The capable fault database and the related maps (Figs. 2-4, 6-7) lay
 507 the foundation for further study of the regional Quaternary faulting and tectonics in the
 508 Israel region. Furthermore, the methodology, which is based on categorisation and sub-
 509 categorisation by seismo-tectonic hierarchic criteria, enables differentiation of hazard
 510 potential and can be applied in other regions around the world.

511

512 **Acknowledgments**

513 We thank the following people for their collaboration and assistance: R. Amit, Y. Avni,
 514 Y. Bartov, Z. Ben-Avraham, G. Baer, M. Beyth, A. Borshevsky, R. Calvo, Y. Eyal, Z.
 515 Garfunkel, H. Ginat, Z. Gvirtzman, Y. Hamiel, S. Hoyland, S. Ilani, R. Kamai, W. Lettis,
 516 T. Levi, D. Mor, C. Netzer, P. Nuriel, Y. Sagy, A. Salomon, A. Sneh, R. Weinberger, E.
 517 Zilberman.

518

519

520 **9. References**

521

- 522 Agnon, A.: Pre-instrumental earthquakes along the Dead Sea Rift, in: Dead Sea
 523 Transform Fault System: Reviews, edited by: Garfunkel, Z., Ben-Avraham, Z., and
 524 Kagan, E. J., Springer, Dordrecht, the Netherlands, 207–262, 2014.
- 525 Aldersons, F., Ben-Avraham, Z., Hofstetter, A., Kissling, E., and Al-Yazjeen, T.: Lower-
 526 crustal strength under the Dead Sea basin from local earthquake data and
 527 rheological modeling, *Earth Planet. Sc. Lett.*, 214, 129–142, 2003.



- 528 Ambraseys, N.: Earthquakes in the Mediterranean and Middle East: a multidisciplinary
 529 study of seismicity up to 1900, Cambridge University Press, New York, 2009.
- 530 Amit, R., Zilberman, E., Enzel, Y. and Porat, N.: Paleoseismic evidence for time
 531 dependency of seismic response on a fault system in the southern Arava Valley,
 532 Dead Sea rift, Israel, *Geol. Soc. Am. Bull.*, 114(2), 192–206, 2002.
- 533 Atkinson, G. M., and Goda, K.: Probabilistic seismic hazard analysis of civil
 534 infrastructure, in: *Handbook of Seismic Risk Analysis and Management of Civil*
 535 *Infrastructure Systems*, edited by: Tesfamariam, S., and Goda, K., 3–28,
 536 <https://doi.org/10.1533/9780857098986.1.3>, 2013.
- 537 Baer, G., Sandwell, D., Williams, S., Bock, Y. and Shamir, G.: Coseismic deformation
 538 associated with the November 1995, Mw= 7.1 Nuweiba earthquake, Gulf of Elat
 539 (Aqaba), detected by synthetic aperture radar interferometry, *J. Geophys. Res.:*
 540 *Solid Earth*, 104(B11), 25221–25232, 1999.
- 541 Bartov, Y.: A Structural and paleogeographical study of the central Sinai faults and
 542 domes, Ph.D. thesis, Hebrew University of Jerusalem, 143 pp. (in Hebrew, English
 543 abstract), 1974.
- 544 Bartov, Y., and Sagy, A.: Late Pleistocene extension and strike-slip in the Dead Sea
 545 Basin, *Geol. Mag.*, 141(5), 565–572, 2004.
- 546 Ellenblum, R., Marco, S., Kool, R., Davidovitch, U., Porat, R., and Agnon, A.:
 547 Archaeological record of earthquake ruptures in Tell Ateret, the Dead Sea Fault,
 548 *Tectonics*, 34, 2105–2117, <https://doi.org/10.1002/2014TC003815>, 2015.
- 549 Eyal, Y., and Reches, Z.: Tectonic analysis of the Dead Sea Rift Region since the Late-
 550 Cretaceous based on mesostructures, *Tectonics*, 2(2), 167–185, 1983.
- 551 Ferry, M., Meghraoui, M., Abou Karaki, N., Al-Taj, M., and Khalil, L.: Episodic
 552 Behavior of the Jordan Valley Section of the Dead Sea Fault Inferred from a 14-ka-
 553 Long Integrated Catalog of Large Earthquakes, *B. Seismol. Soc. Am.*, 101(1), 39–
 554 67, <https://doi.org/10.1785/0120100097>, 2011.



- 555 Galadini, F., Falcucci, E., Galli, P., Giaccio, B., Gori, S., Messina, P., Moro, M., Saroli,
 556 M., Scardia, G. and Sposato, A.: Time intervals to assess active and capable faults
 557 for engineering practices in Italy, *Eng. Geol.*, 139, 50–65, 2012.
- 558 Garfunkel, Z.: Internal structure of the Dead Sea leaky transform (rift) in relation to plate
 559 kinematics, in: *The Dead Sea Rift*, edited by: Freund, R., Garfunkel, Z.,
 560 *Tectonophysics*, 80, 81–108, 1981.
- 561 Garfunkel, Z.: Constrains on the origin and history of the Eastern Mediterranean basin,
 562 *Tectonophysics*, 298, 5–35, 1998.
- 563 Garfunkel, Z.: The long- and short-term lateral slip and seismicity along the Dead Sea
 564 Transform: An interim evaluation, *Israel J. Earth. Sci.*, 58(3), 217–235,
 565 <https://doi.org/10.1560/IJES.58.3-4.217>, 2011.
- 566 Garfunkel, Z.: Lateral motion and deformation along the Dead Sea transform, in: *Dead*
 567 *Sea Transform Fault System: Reviews*, edited by: Garfunkel, Z., Ben-Avraham, Z.,
 568 and Kagan, E. J., Springer, Dordrecht, the Netherlands, 109–150, 2014.
- 569 Garfunkel, Z., and Bartov, Y.: The tectonics of the Suez rift, *Geological Survey of Israel*
 570 *Bulletin*, 71, 1–44, 1977.
- 571 Garfunkel, Z., and Ben-Avraham, Z.: Basins along the Dead Sea transform, *Mémoires*
 572 *du Muséum national d’histoire naturelle*, 186, 607–627, 2001.
- 573 Gomez, F., Meghraoui, M., Darkal, A. B., Hijazi, F., Mouty, M., Suleiman, Y., Sbeinati,
 574 R., Darawcheh, R., Al-Ghazzi, R., and Barazabgi, M.: Holocene faulting and
 575 earthquake recurrence along the Serghaya branch of the Dead Sea Fault system in
 576 Syria and Lebanon, *Geophys. J. Int.*, 153, 658–674, 2003.
- 577 Gomez, F., Karam, G., Khawlie, M., McClusky, S., Vernant, P., Reilinger, R., R., Jaafar,
 578 R., Tabet, C., Khair, K., and Barazangi, M.: Global Positioning System
 579 measurements of strain accumulation and slip transfer through the restraining bend
 580 along the Dead Sea fault system in Lebanon, *Geophys. J. Int.*, 168(3), 1021–1028,
 581 2007.



- 582 Hamiel, Y., Piatibratova, O., and Mizrahi, Y.: Creep along the northern Jordan Valley
 583 section of the Dead Sea Fault, *Geophys. Res. Lett.*, 43(6), 2494–2501, 2016.
- 584 Hamiel, Y., Masson, F., Piatibratova, O., and Mizrahi, Y.: GPS measurements of crustal
 585 deformation across the southern Arava Valley section of the Dead Sea Fault and
 586 implications to regional seismic hazard assessment, *Tectonophysics*, 724–725, 171–
 587 178, <https://doi.org/10.1016/j.tecto.2018.01.016>, 2018a.
- 588 Hamiel, Y., Piatibratova, O., Mizrahi, Y., Nahmias, Y., and Sagy, A.: Crustal
 589 deformation across the Jericho Valley section of the Dead Sea Fault as resolved by
 590 detailed field and geodetic observations, *Geophys. Res. Lett.*, 45, 3043–3050,
 591 <https://doi.org/10.1002/2018GL077547>, 2018b.
- 592 Heimann, A.: Active faulting in Israel, Geological Survey of Israel Report No.
 593 GSI/07/02, Jerusalem, 33 pp. (in Hebrew), 2002.
- 594 Hofstetter, A., van Eck, T., and Shapira, A.: Seismic activity along fault branches of the
 595 Dead Sea-Jordan transform system: the Carmel – Tirza fault system,
 596 *Tectonophysics*, 267, 317–330, 1996.
- 597 Hofstetter, A., Thio, H. K., and Shamir, G.: Source mechanism of the 22/11/1995 Gulf of
 598 Aqaba earthquake and its aftershock sequence, *J. Seismol.*, 7, 99–114, 2003.
- 599 Hofstetter, R., Klinger, Y., Amrat, A.-Q., Rivera, L., and Dorbath, L.: Stress tensor and
 600 focal mechanisms along the Dead Sea fault and related structural elements based on
 601 seismological data, *Tectonophysics*, 429, 165–181, 2007.
- 602 Hofstetter, R., Gitterman, Y., Pinsky, V., Kraeva, N., and Feldman, L.: Seismological
 603 observations of the northern Dead Sea basin earthquake on 11 February 2004 and
 604 its associated activity, *Isr. J. Earth Sci.*, 57, 101–124, 2008.
- 605 International Atomic Energy Agency (IAEA): Seismic Hazards in Site Evaluation for
 606 Nuclear Installations Specific Safety Guide: IAEA Safety Standards Series No.
 607 SSG-9, International Atomic Energy Agency, Vienna, 2010.
- 608 IEC and WLA (Israel Electric Corporation and William Lettis & Associates, Inc.):
 609 Shivta-Rogem Site Report. Israel Electric Corporation, Ltd., 2002.



- 610 Jaeger, J. C., Cook, N. G. W., and Zimmerman, R. W.: Fundamentals of Rock Mechanics
 611 (4th ed.), Blackwell, Malden, Mass., 488 pp., 2007.
- 612 Joffe, S., and Garfunkel, Z.: Plate kinematics of the circum Red Sea – a re-evaluation, in:
 613 Sedimentary Basins within the Dead Sea and Other Rift Zones, edited by: Ben-
 614 Avraham, Z., Tectonophysics, 141, 5-22, 1987.
- 615 Klinger, Y., Le Béon, M. and Al-Qaryouti, M.: 5000 yr of paleoseismicity along the
 616 southern Dead Sea fault, Geophys. J. Int., 202(1), pp.313–327, 2015.
- 617 Mai, M., and Beroza, G. C.: Source scaling properties from finite-fault-rupture models.
 618 B. Seismol. Soc. Am., 90(3), 604–615, 2000.
- 619 Marano, K. D., Wald, D. J., and Allen, T. I.: Global earthquake casualties due to
 620 secondary effects: a quantitative analysis for improving rapid loss analyses, Nat.
 621 Hazards, 52, 319–328, 2010.
- 622 Marco, S., Rockwell, T. K., Heimann, A., Frieslander, U., and Agnon, A.: Late Holocene
 623 activity of the Dead Sea transform revealed in 3D palaeoseismic trenches on the
 624 Jordan Gorge Segment, Earth Planet. Sc. Lett., 234, 189–205, 2005.
- 625 Marco, S.: Recognition of earthquake-related damage in archaeological sites: Examples
 626 from the Dead Sea fault zone, Tectonophysics, 453(1–4), 148–156, 2008.
- 627 Marco, S., and Klinger, Y.: Review of on-fault palaeoseismic studies along the Dead Sea
 628 fault, in: Dead Sea Transform Fault System: Reviews, edited by: Garfunkel, Z.,
 629 Ben-Avraham, Z., and Kagan, E. J., Springer, Dordrecht, the Netherlands, 183–205,
 630 2014.
- 631 Masson, F., Hamiel, Y., Agnon, A., Klinger, Y., and Deprez, A.: Variable behavior of the
 632 Dead Sea Fault along the southern Arava segment from GPS measurements, C. R.
 633 Geosci., 347, 161–169, 2015.
- 634 McKenzie, D. P.: Plate tectonics of the Mediterranean Region, Nature, 226, 239–243,
 635 1970.
- 636 Meghraoui, M., Gomez, F., Sbeinati, R., Van der Woerd, J., Mouty, M., Darkal, A. N.,
 637 Radwan, Y., Layyous, I., Al Najjar, H., Darawcheh, R., Hijazi, F., Al-Ghazzi, R.,



- 638 and Barazangi, M.: Evidence for 830 years of seismic quiescence from
 639 palaeoseismology, archaeoseismology and historical seismicity along the Dead Sea
 640 fault in Syria, *Earth Planet. Sc. Lett.*, 210, 35–52, 2003.
- 641 Meirova, T., and Hofstetter, A.: Observations of seismic activity in Southern Lebanon, J.
 642 *Seismol.*, 17(2), 629–644, 2013.
- 643 Neev, D., Almador, G., Arad, A., Ginzburg, A., and Hall, J. K.: The geology of the
 644 southeastern Mediterranean Sea, *Geological Survey of Israel Bulletin*, 68, 1–51,
 645 1976.
- 646 Nemer, T., and Meghraoui, M.: Evidence of coseismic ruptures along the Roum fault
 647 (Lebanon): a possible source for the AD 1837 earthquake, *J. Struct. Geol.*, 28,
 648 1483–1495, 2006.
- 649 Palano, M., Imprescia, P., and Gresta, S.: Current stress and strain-rate fields across the
 650 Dead Sea Fault System: Constraints from seismological data and GPS observations,
 651 *Earth Planet. Sc. Lett.*, 369, 305–316, 2013.
- 652 Picard, L.: The geological evolution of the Quaternary in the central-northern Jordan
 653 Graben, Israel, *Geol. S. Am. S.*, 84, 337–366, 1965.
- 654 Porat, N., Wintle, A.G., Amit, R., and Enzel, Y.: Late Quaternary earthquake chronology
 655 from luminescence dating of colluvial and alluvial deposits of the Arava valley,
 656 Israel, *Quaternary Res.*, 46, 107–117, 1996.
- 657 Quennell, A. M.: Tectonics of the Dead Sea rift, in: *Int. Geol. Congr.*, 20th, Mexico:
 658 *Assoc. Serv. Geol. Afr.*, 385–405, 1959.
- 659 Ron, H. and Eyal, Y.: Intraplate deformation by block rotation and mesostructures along
 660 the Dead Sea transform, northern Israel, *Tectonics*, 4(1), 85–105, 1985.
- 661 Sadeh, M., Hamiel, Y., Ziv, A., Bock, Y., Fang, P., and Wdowinski, S.: Crustal
 662 deformation along the Dead Sea Transform and the Carmel Fault inferred from 12
 663 years of GPS measurements, *J. Geophys. Res.*, 117, B08410,
 664 doi:10.1029/2012JB009241, 2012.



- 665 Sagy, A., Reches, Z. E. and Agnon, A.: Hierarchic three-dimensional structure and slip
 666 partitioning in the western Dead Sea pull-apart, *Tectonics*, 22(1), 2003.
- 671 Sagy, A., Sneh, A., Rosenshaft, M., and Bartov, Y.: Map of 'active' and 'potentially active'
 672 faults that rupture the surface in Israel: Updates 2013 for Israel Standard 413,
 673 Geological Survey of Israel Report No. GSI/02/2013, Jerusalem, 17 pp. (in
 674 Hebrew, English abstract), 2013.
- 675 Sagy, A., Wieler, N., Avni, Y., Rosenshaft, M., and Amit, R.: Map of active and
 676 potentially active faults that rupture the surface in Israel: Updates 2017 for Israel
 677 Standard 413, Geological Survey of Israel Report No. GSI/13/2017, Jerusalem, 19
 678 pp. (in Hebrew, English abstract), 2017.
- 679 Salamon, A., Rockwell, T., Ward, S. N., Guidoboni, E. and Comastri, A.: Tsunami
 680 hazard evaluation of the eastern Mediterranean: historical analysis and selected
 681 modelling, *B. Seismol. Soc. Am.*, 97(3), 705–724, 2007.
- 682 Schattner, U., and Weinberger, R.: A mid-Pleistocene deformation transition in the Hula
 683 basin, northern Israel: Implications for the tectonic evolution of the Dead Sea Fault,
 684 *Geochem. Geophys. Geosy.*, 9(7), Q07009, doi: 10.1029/2007GC001937, 2008.
- 685 Shaked, Y., Agnon, A., Lazar, B., Marco, S., Avner, U., and Stein, M.: Large earthquakes
 686 kill coral reefs at the north- west Gulf of Aqaba, *Terra Nova*, 16(3), 133–138,
 687 2004.
- 688 Shalev, E., Lyakhovsky, V., Yechieli, Y.: Is advective heat transport significant at the
 689 Dead Sea basin?, *Geofluids*, 7, 292–300, 2007.
- 690 Shalev, E., Lyakhovsky, V., Weinstein, Y., and Ben-Avraham, Z.: The thermal structure
 691 of Israel and the Dead Sea Fault, *Tectonophysics*, 602, 69–77, 2013.
- 692 Shapira, A., and Hofstetter, A.: Source parameters and scaling relationships of
 693 earthquakes in Israel, *Tectonophysics*, 217, 217–226, 1993.
- 694 Sneh, A., Bartov, Y., Weissbrod, T., and Rosenshaft, M.: Geological Map of Israel,
 695 1:200,000 (4 sheets), Geological Survey of Israel, Jerusalem, 1998.



- 696 Steckler, M. S., Berthelot, F., Lyberis, N., and Le Pichon, X.: Subsidence in the Gulf of
697 Suez: implications for rifting and plate kinematics, *Tectonophysics*, 153, 249–270,
698 1988.
- 699 Stirling, M., Rhoades, D., and Berryman, K.: Comparison of Earthquake Scaling
700 Relations Derived from Data of the Instrumental and Preinstrumental Era, *B.*
701 *Seismol. Soc. Am.*, 92(2), 812–830, 2002.
- 702 Stirling, M., Goded, T., Berryman, K. and Litchfield, N.: Selection of earthquake scaling
703 relationships for seismic- hazard analysis. *B. Seismol. Soc. Am.*, 103(6), 2993–
704 3011, 2013.
- 705 ten Brink, U. S., and Flores, C. H.: Geometry and subsidence history of the Dead Sea
706 basin: A case for fluid induced mid-crustal shear zone? *J. Geophys. Res.*, 117,
707 B01406, doi:10.1029/2011JB008711, 2012.
- 708 Torfstein, A., Haase-Schramm, A., Waldmann, N., Kolodny, Y., and Stein, M.: U-series
709 and oxygen isotope chronology of the mid-Pleistocene Lake Amora (Dead Sea
710 basin), *Geochim. Cosmochim. Ac.*, 73(9), 2603–2630, 2009.
- 711 Wells, D. L., and Coppersmith, K. J.: New empirical relationships among magnitude,
712 rupture length, rupture width, rupture area, and surface displacement, *B. Seismol.*
713 *Soc. Am.*, 84(4), 974–1002, 1994.
- 714 Wetzler, N., and Kurzon, I.: The earthquake activity in Israel: Revisiting 30 years of local
715 and regional seismic records along the Dead Sea transform, *Seismol. Res. Lett.*,
716 87(1), 47–58, 2016.
- 717 Wetzler, N., Sagy, A. and Marco, S.: The association of micro- earthquake clusters with
718 mapped faults in the Dead Sea basin, *J. Geophys. Res.: Solid Earth*, 119(11), 8312–
719 8330, 2014.
- 720 Woo, G.: Kernel estimation methods for seismic hazard area source modelling, *B.*
721 *Seismol. Soc. Am.*, 86(2), 353–362, 1996.
- 722 Zilberman, E., Greenbaum, N., Nahmias, Y., and Porat, N.: The evolution of the northern
723 shutter ridge, Mt. Carmel, and its implications on the tectonic activity along the



- 724 Yagur fault, Geological Survey of Israel Report No. GSI/14/2011, Jerusalem, 25
725 pp., 2011.
- 726 Zoback, M. L.: First-and second-order patterns of stress in the lithosphere: The World
727 Stress Map Project, J. Geophys. Res.: Solid Earth, 97(B8), 11703–11728, 1992.
- 728



729 **Table 1: Main strike-slip faults: average slip rate details**

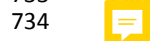
| Fault | Strike-slip [mm/yr] | Data | Period | Reference |
|---|--------------------------|-------------------------------|------------------------|---|
| Aragonese [ARF] | ~5* | GPS | Recent | Baer et al. 1999; Hamiel et al., 2018a |
| Arava [AF] | ~4.9# | GPS | Recent | Masson et al., 2015 |
| Evrona [EF] | 5.0±0.8# | GPS | Recent | Hamiel et al., 2018a |
| Jericho [JF] | 4.8±0.7#! | GPS | Recent | Hamiel et al., 2018b |
| Jordan Valley [JVF] (central) | ~5# | Geology | ~25ka | Ferry et al., 2011 |
| Jordan Valley (South to Sea of Galilee) | 4.1±0.8#& | GPS | Recent | Hamiel et al., 2016 |
| Jordan Gorge | 4.1±0.8# ~3# ~2.6# | GPS Geology Archaeology | Recent ~5ka ~3ka | Hamiel et al., 2016 Marco et al., 2005 Ellenblum et al., 2015 |
| Lebanon Restraining Bend (LRB) | 3.8±0.3* | GPS | Recent | Gomez et al., 2007 |
| Qiryat Shemona | 3.9±0.3*! | GPS | Recent | Gomez et al., 2007 |
| Roum | 0.86–1.05# | Geology | Holocene | Nemer and Meghraoui, 2006 |
| Serghaya | 1.4±0.2# | Geology | Holocene | Gomez et al., 2003 |
| Yammuneh (LRB – northern part) | 2.8±0.5 | GPS | Recent | Gomez et al., 2003; 2007 |
| Yammuneh (north of LRB) | 6.9±0.1# 4.2±0.3* | Geology GPS | 2ka Recent | Meghraoui et al., 2003 Gomez et al., 2007 |

730 # Geodetic or geological measurements on a specific segment.

731 ! 0.8 mm/yr of extension normal to the fault

732 * According to geodetic-based model

733 & Partially creeping





735 **Table 2. Marginal faults and branches with integrated slip or subsidence of ~ 0.5 mm/yr**
 736 **$\leq VS \leq \sim 1$ mm/yr and references**

| Fault | Slip rate [mm/yr] | Data | Period | Reference |
|--------------------------------------|--|-----------------------|----------------------|---|
| Dead Sea basin marginal faults | ≥ 1 Based on basin subsidence rates | Geology Geophysics | Pleistocene-Holocene | Torfstein et al., 2009; ten Brink and Flores, 2012; Bartov and Sagy, 2004 |
| Carmel-Tirza-Izrael fault zone [CTF] | 0.9 ± 0.45 total slip rate (0.7 ± 0.45 lateral; 0.6 ± 0.45 extension) | GPS | Recent | Sadeh et al., 2012 |
| Carmel | < 0.5 | Geology | 200ka | Zilberman et al., 2011 |
| Hula western border | > 0.4 Based on basin subsidence rates | Geology Geophysics | ~ 1 Ma | Schattner and Weinberger, 2008 |
| Elat | ? | Geology | Holocene | Amit et al., 2002; Porat et al., 1996; Shaked et al., 2004 |

737



738 Figure captions

739 **Figure 1: Plate configuration in the Eastern Mediterranean. Arrows show relative motion.**
 740 **SR-Suez Rift; GEA: Gulf of Elat/Aqaba. DST-Dead Sea Transform fault system; CTF-**
 741 **Carmel Tirza Fault zone; LRB-Lebanon Restraining Bend; CA- Cyprian Arc.**

742 **Figure 2: Epicentres in Israel and surrounding areas between the years 1983-2017, based on**
 743 **the relocated earthquake catalogue. Circle size and colours indicate the magnitude. Black**
 744 **lines represent the main fault segments of the DST and the CTF. The background for this**
 745 **figure and the followings is based on Farr et al., (2007).**

746 **Figure 3: The earthquake kernel density distribution, according to the relocated catalogue.**
 747 **Colours and corresponding numbers indicate the value in [events/km²/yr].**

748 **Figure 4: The seismic moment kernel density distribution, according to the *relocated***
 749 ***catalogue. Colours and corresponding numbers indicate the value in log[joule/km²/yr].***

750 **Figure 5: The main seismic sources in Israel and adjacent areas. Colours indicate the two**
 751 **categories of faults according to the criteria. Inferred subsurface faults are marked by**
 752 **dashed lines. Abbreviations are for the DST main strike-slip segments, its main branches**
 753 **and marginal faults. Numbers indicate geodetic slip rates [mm/yr] for strike-slip**
 754 **components, according to recent studies (Tables 1, 2).**

755 **Figure 6. The seismicity polygons: earthquake density of values > ~0.001[events/km²/yr] and**
 756 **Mo density of values > ~9.5 log[joule/km²/yr]; the product is the overlap polygon (in**
 757 **brown).**

758 **Figure 7. Quaternary fault map of Israel. Colours indicate the corresponding criterion for**
 759 **each fault. Inferred subsurface faults are marked by dashed lines. Abbreviations are for the**
 760 **main strike-slip segments of the DST.**

761

762

763

764

765

766

767



768

769 **Figure 1**

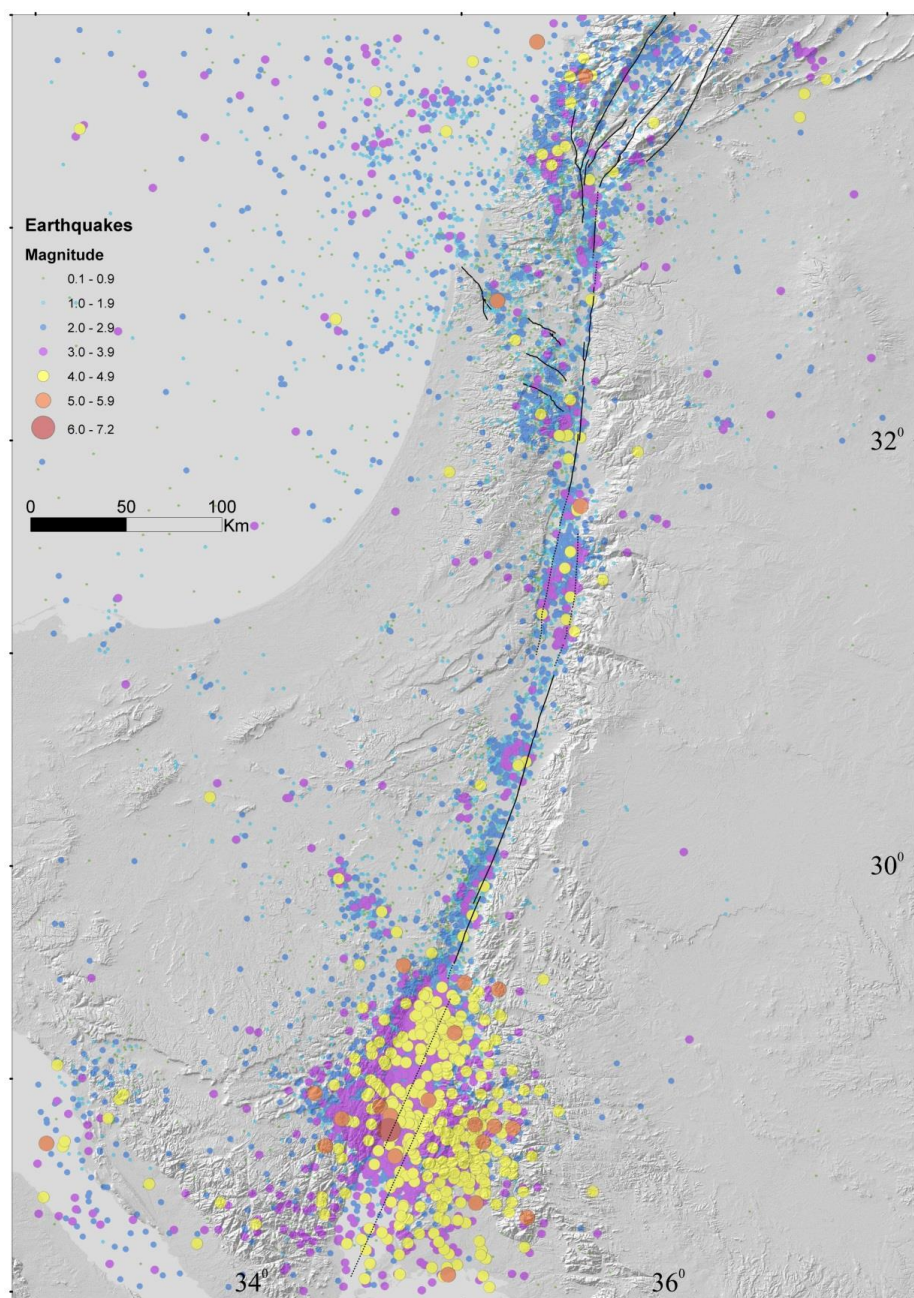
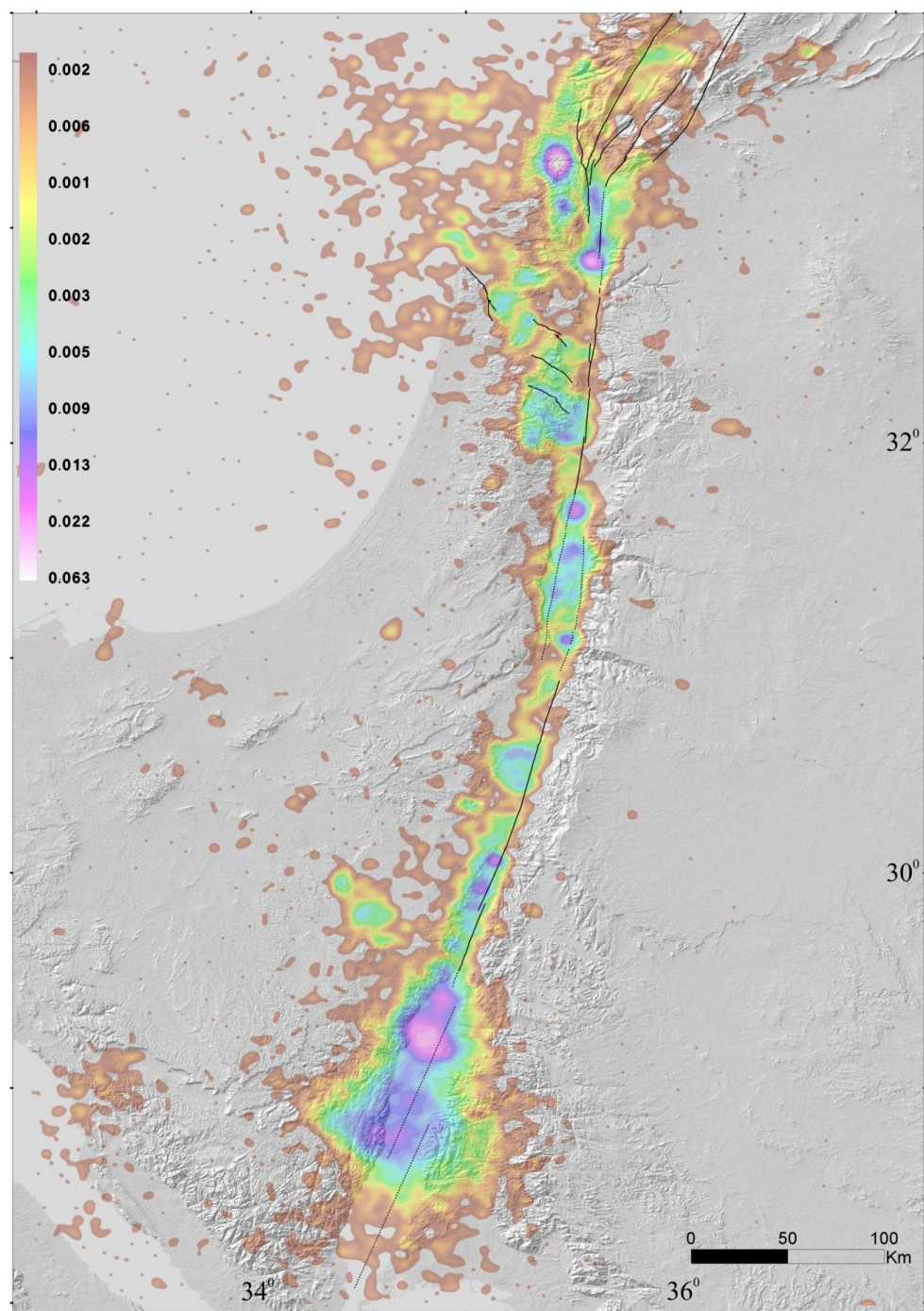


Figure 2



773

774 **Figure 3**

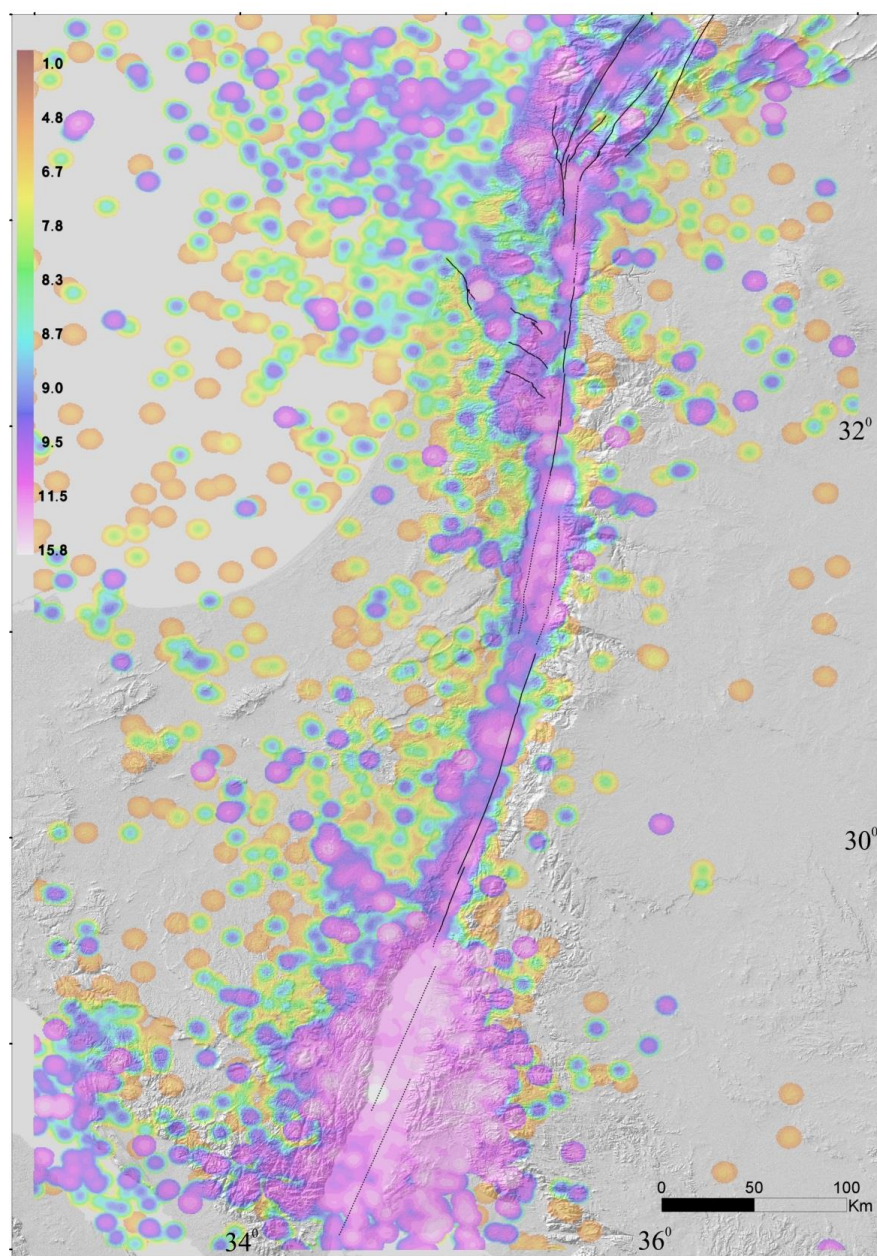


Figure 4

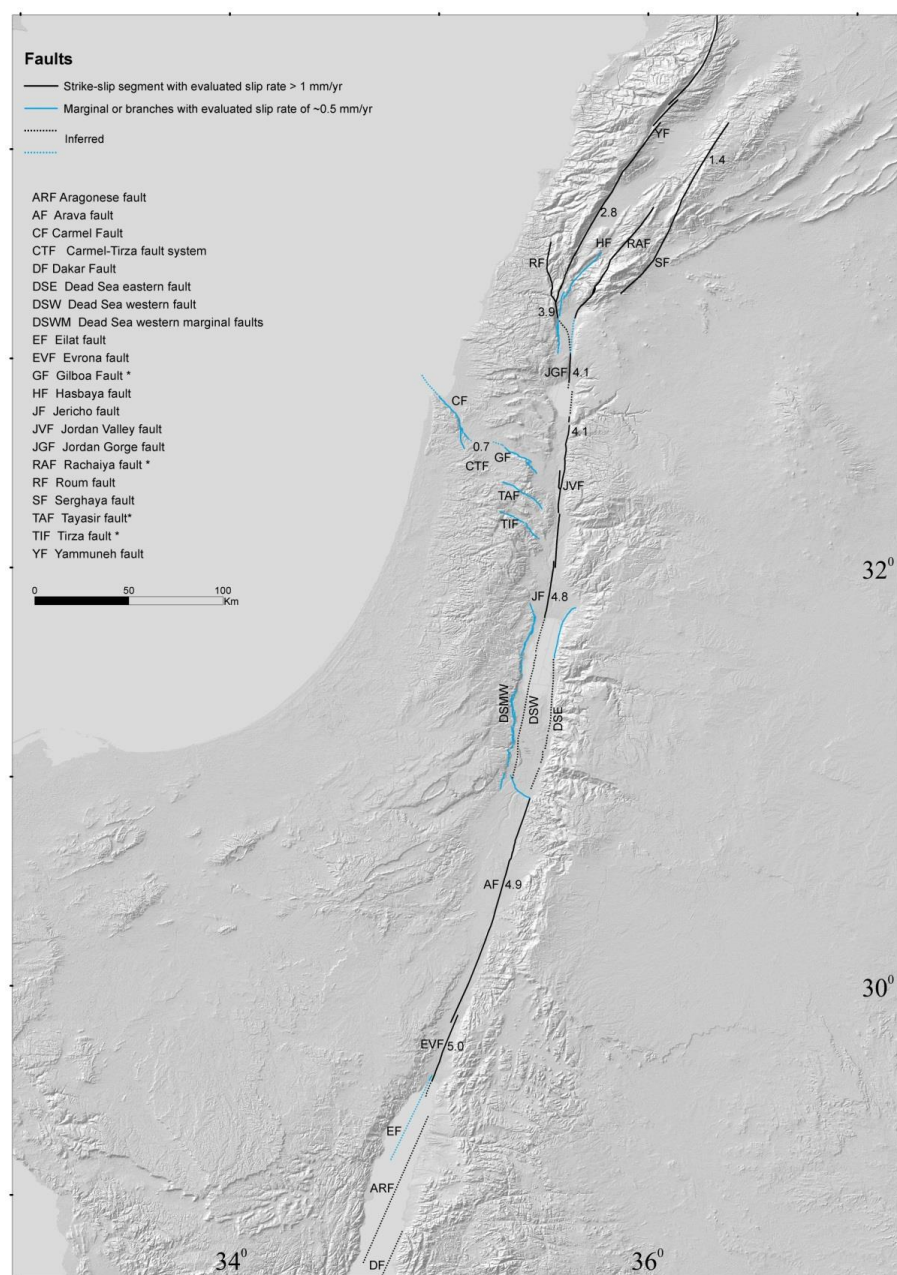


Figure 5

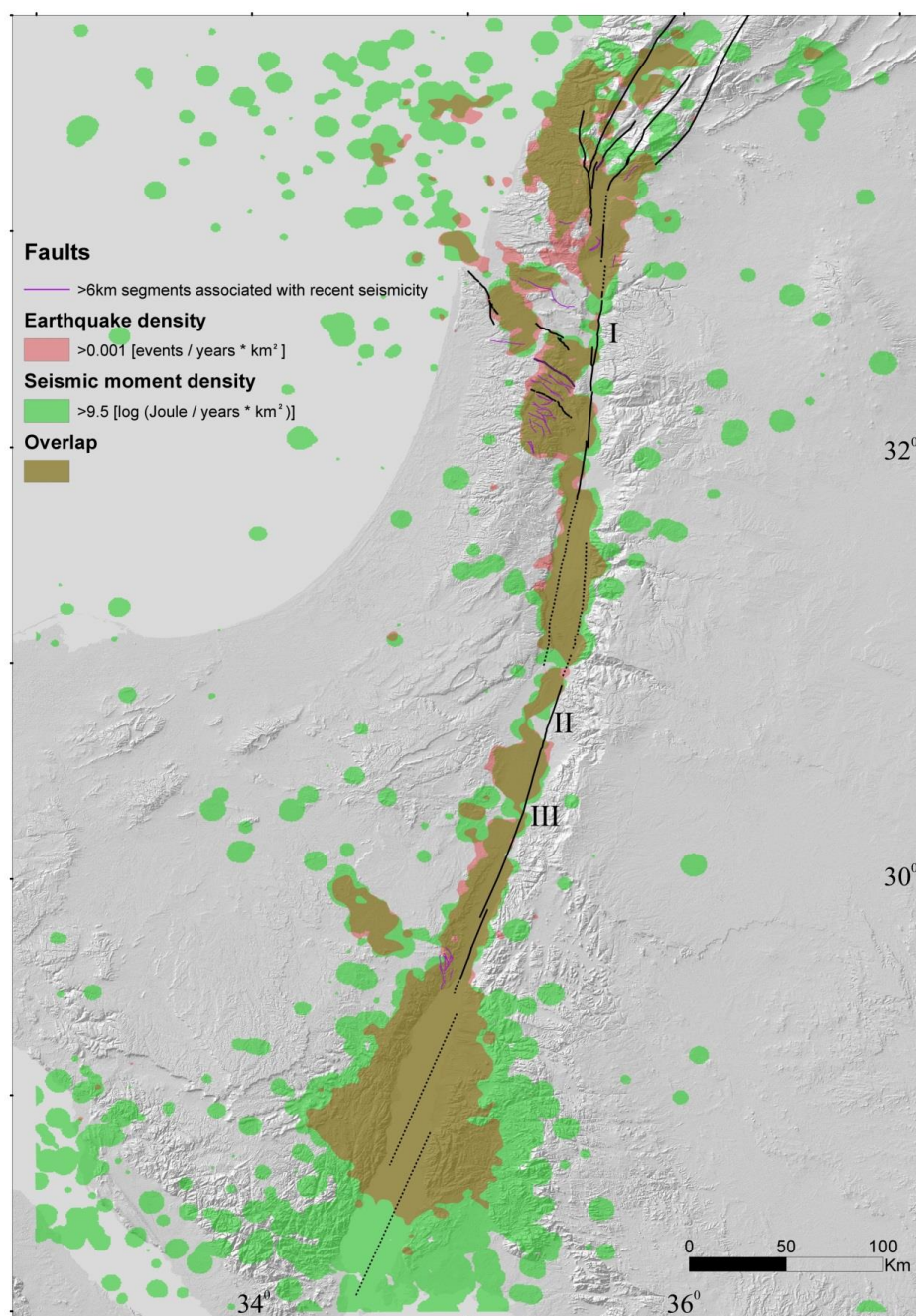
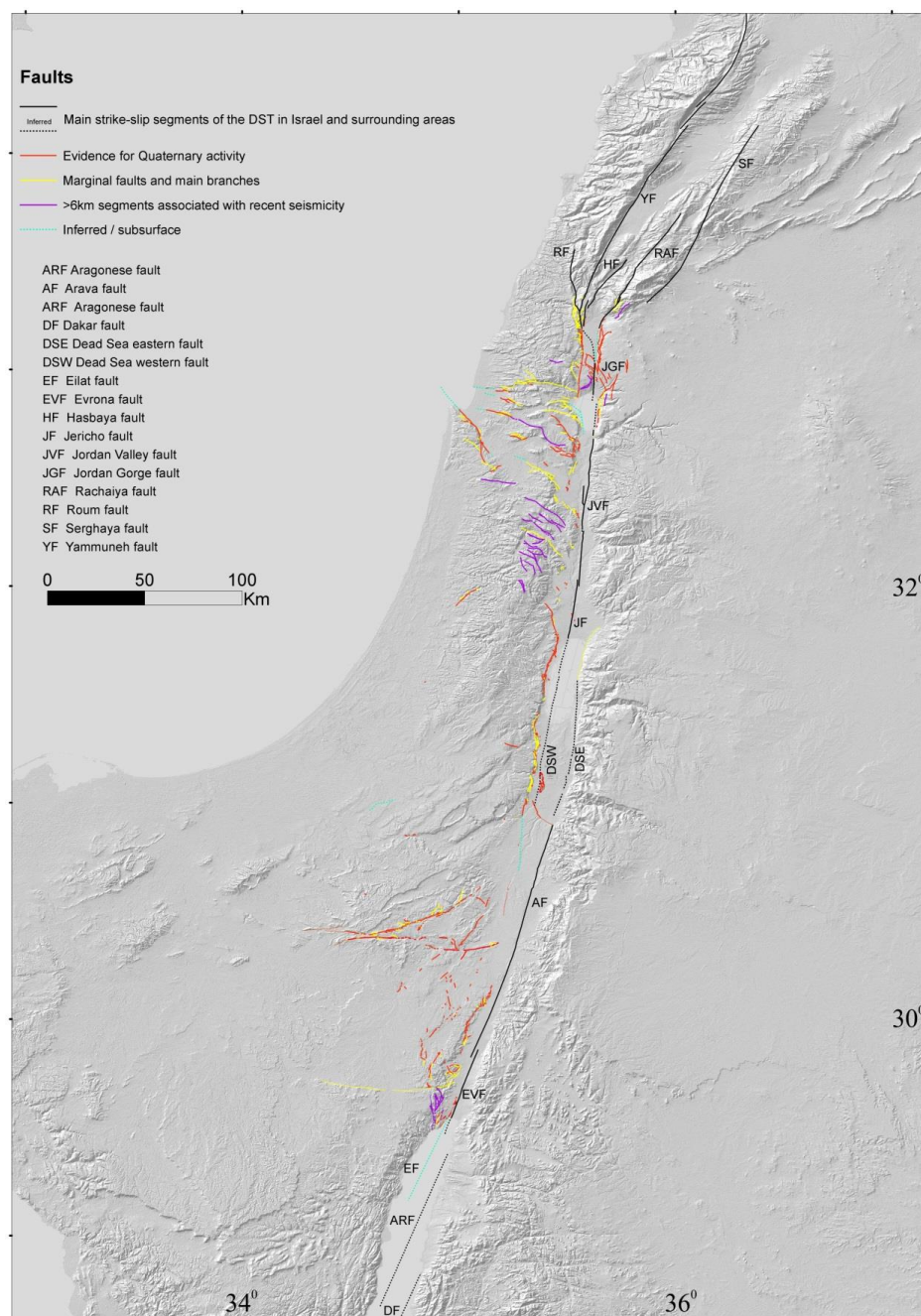


Figure 6



786

787 **Figure 7**



788 **Appendix 1**

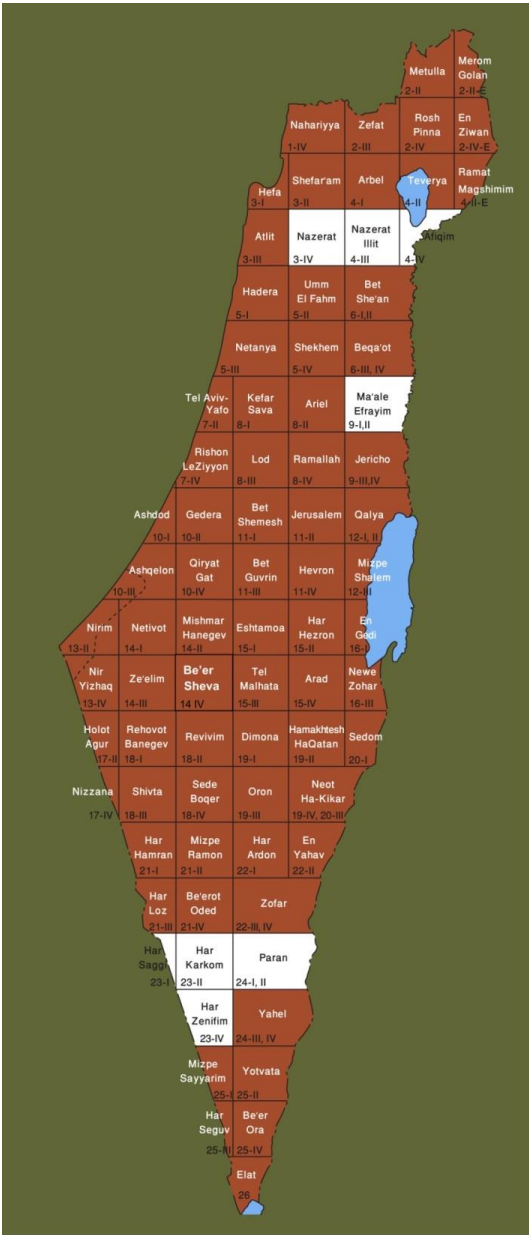


Figure A1. Locations of the 1:50,000 geological map sheets used for the present map (as of August 2018). Brown: locations of published 1:50,000 sheets. White: unpublished sheets.



795 **Table A1: References for faults and fault segments that have been marked based on**
 796 **papers, reports, and theses. Faults are listed in table 3 if their latest mapping is not**
 797 **updated yet in the 1:50,000 sheets (as of 2018), or if their definition as Quaternary**
 798 **faults cannot be directly deduced from the geological maps. Fault names are mainly**
 799 **according to the references.**

800

| Area | Name of fault / group of faults or segments | References |
|---|---|--|
| Southern Israel | Arif-Bator | Zilberman et al., 1996; Avni, 1998 |
| | Gerofit | Ginat, 1997 |
| | Gevaot Ziya | Avni, 1998 |
| | Halamish line | Avni, 1998 |
| | Har Seguv | Avni, 1998 |
| | Hiyyon | Ginat, 1997 |
| | Katzra | Avni, 1998 |
| | Milhan | Ginat, 1997 |
| | Mitzpe Sayarim | Avni, 1998 |
| | Noza | Ginat, 1997 |
| | Ovda | Avni, 1998 |
| | Paran | Zilberman, 1985; Avni, 1998; Calvo et al., 1998; Calvo, 2002 |
| | Yotam | Wieler et al., 2017 |
| | Zhiha | Avni, 1998 |
| | Zin | Enzel et al., 1988; IEC and WLA, 2002; Avni and Zilberman, 2007 |
| | Znifim – Zihor – Barak | Ginat, 1997 |
| | Zofar | Calvo, 2002 |
| Central Israel and Dead Sea area | Jericho | Sagy and Nahmias, 2011 |
| | Masada Plain | Bartov et al., 2006 |
| | Modi'in | Buchbinder and Sneh, 1984 |
| | Nahal Darga (east) | Enzel et al., 2000 |
| | Nahal Kidron (east) | Sagy and Nahmias, 2011 |
| Northern Israel | Ahihud | Kafri and Ecker, 1964; Zilberman et al., 2011 |
| | Beit Qeshet (western part) | Zilberman et al., 2009 |
| | Ha'on | Katz et al., 2009 |
| | Hilazon | Kafri and Ecker, 1964; Zilberman et al., 2008 |
| | Kabul | Kafri and Ecker, 1964; Zilberman et al., 2008 |
| | Nahef East Fault | Mitchell et al., 2001 |
| | Nesher | Zilberman et al., 2006; 2008 |
| | Tiberias | Marco et al., 2003 |

801

802



803 **Table A2: List of geological formations and units used for the QFMI Geologic and**
 804 **geomorphic descriptions that appear in 1:50,000 geological maps for Quaternary**
 805 **deposits.**

806

| Formations | Local sedimentary units | Local volcanic units | Other units* |
|-------------------------|-------------------------|--|---|
| Ahuzam Fm. (Cgl.) | Amora Salt | Avital Tuff | Alluvium |
| Arava Fm. | Betlehem Cgl. | Bene Yehuda Scoria | Beach rocks & reefs |
| Amora Fm. | Biq'at Uvda Cgl. | Brekhat Ram Tuff | Calcareous sandstone (kurkar) |
| Ashmura Fm. | Edom facias | Dalton Basalt | Colluvium |
| Garof Fm. | Egel Cgl. | Dalton Scoria & Tuff | Dune sand, Sand sheets, Red sands |
| Gesher Bnot Ya'akov Fm. | En Awwazim Cgl. | Dalwe flows | Loess, fluvial & eolian |
| Hazor & Gadot Fms. | En Feshha Cgl. | En Awwazim flow | Gypsum |
| Lisan Fm. | Giv'at Oz Cgl. | En Zivan Basalt flows | Lake sediments |
| Malaha Fm. | Karbolet caprock | Golan Basalt flows (Muweissa and En Zivan flows) | Loam (hamra) |
| Mazar Fm. | Lot caprock | Hazbani Basalt flows | Neogene-Quaternary conglomerate units, Terrace cgl. |
| Nevatim Fm. | Mahanayim Marl | Keramim Basalt | Playa |
| Ortal Fm. | Mearat Sedom caprock | Meshki Basalt flows | Recent fan |
| Pleshet Fm. | Nahshon Cgl. | Muweisse Basalt flows | Soil |
| Samra Fm. | Ramat Geroft Cgl. | Neogene Basalts | Tufa, travertine |
| Sede Zin Fm. | Ravid Cgl. | Raqad Basalt | Unnamed clastic unit |
| Seif Fm. | Ruhama Loess & sand | Sa'ar Basalt flows | |
| Ye'elim Fm. | Sabkha soil | Shievan Scoria | |
| Ze'elim Fm. | Si'on Cgl. | Yarda/Ruman Basalt flows | |
| Zehiha Fm. | Wadi Malih Cgl. | Yarmouk Basalt | |
| | | Yehudiyya & Dalwe Basalt flows | |

807



808

809 **Table A3: References for faults located beyond Israel borders and/or subsurface faults**

| Geographic area | Reference |
|-----------------------------|--|
| Gulf of Elat | Ben-Avraham, 1985; Hartman et al., 2014; |
| Arava valley | Calvo, 2002; Le Béon et al., 2012; Sneh and Weinberger, 2014 |
| Sinai peninsula | Sneh and Weinberger, 2014 |
| North-western Negev | Eyal et al., 1992 |
| Dead Sea basin | Ben-Avraham and Schubert, 2006; Sneh and Weinberger, 2014 |
| Jordan valley | Ferry et al., 2007; Sneh and Weinberger, 2014 |
| Gilboa fault (western part) | Sneh and Weinberger, 2014 |
| Carmel fault (eastern part) | Sneh and Weinberger, 2014 |
| Carmel fault (western part) | Schattner and Ben-Avraham, 2007 |
| Zvulun Valley | Sagy and Gvirtzman, 2009 |
| Sea of Galilee | Hurwitz et al., 2002; Reznikov et al., 2004; Eppelbaum et al., 2007; Sneh and Weinberger, 2014 |
| Hula basin | Schattner and Weinberger, 2008 |
| Lebanon and Syria | Weinberger et al., 2009; Garfunkel, 2014; Sneh and Weinberger, 2014 |

810 *Table A3: References for faults located beyond Israel borders and/or subsurface faults*

811

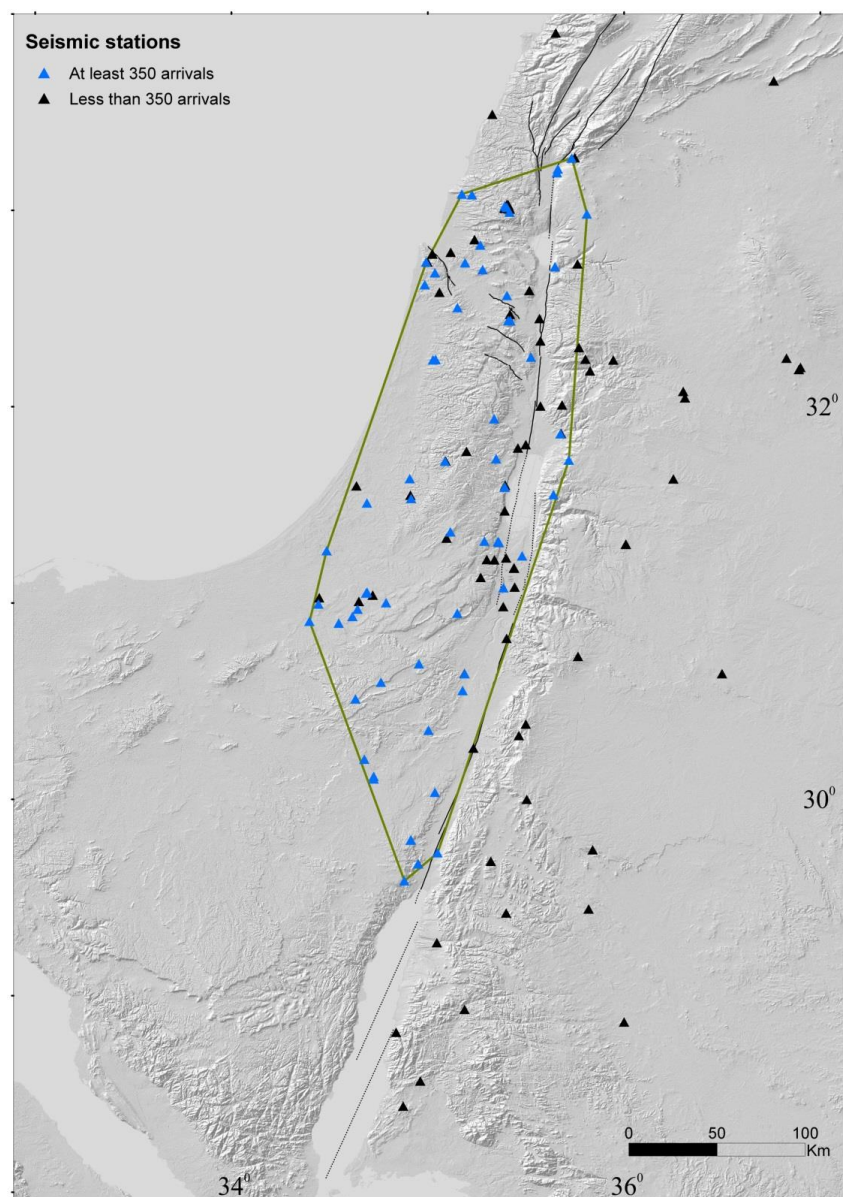


Figure A2. Seismic stations utilised for recording the earthquakes of the examined catalogue, and the ensuing seismic network coverage area. The spatial distribution of the stations is temporal dependent. Stations that recorded less than 350 arrivals are in black, while stations that recorded more than 350 arrivals are in blue. Green lines mark the borders of the seismic network coverage area as defined in this study.

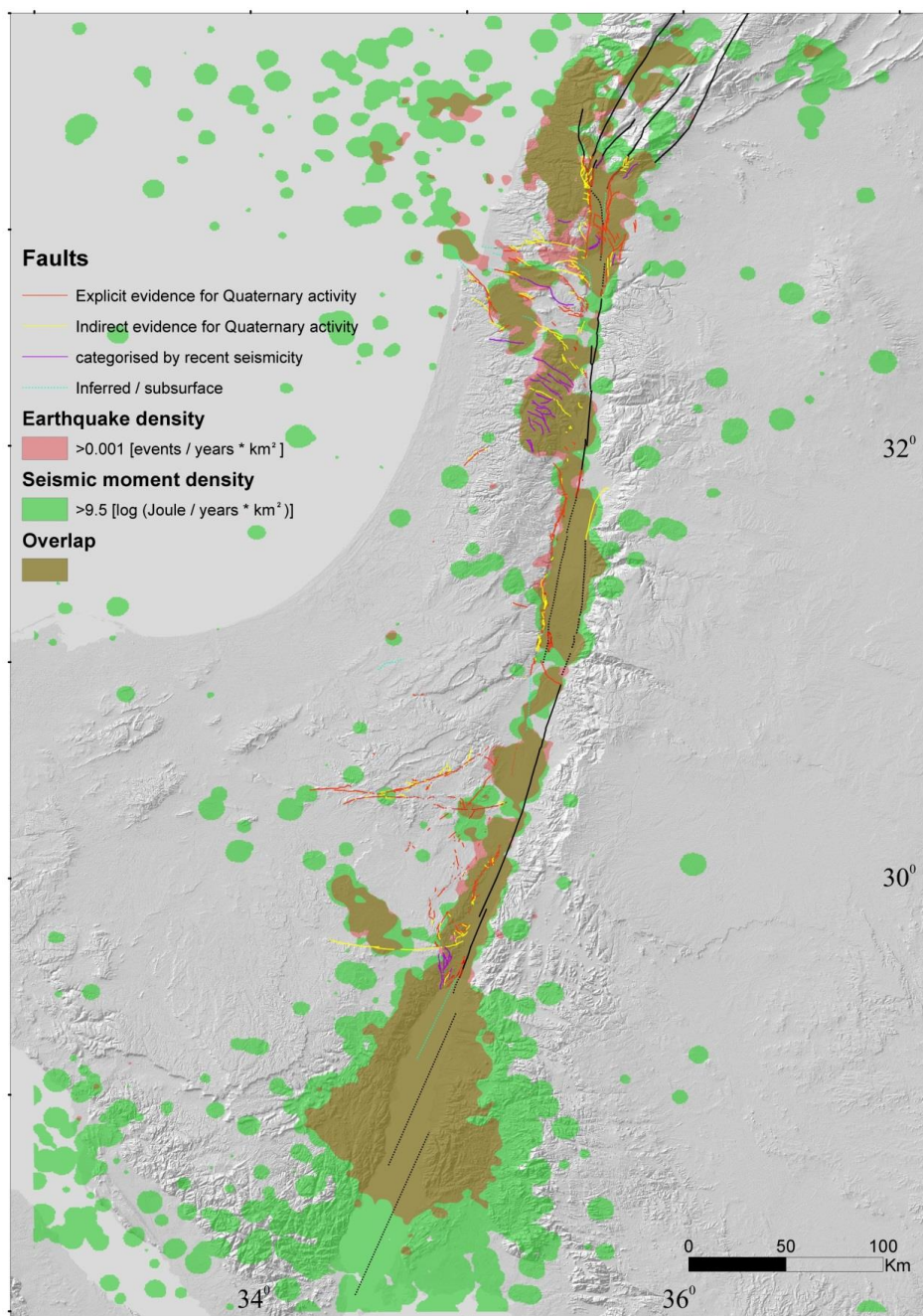


Figure A3. Quaternary faults superimposed on the seismicity polygons of the seismicity-based criterion.



823 **10. Appendix references**

- 824 Avni, Y.: Paleogeography and tectonics of the Central Negev and the Dead Sea Rift
 825 western margin during the late Neogene and Quaternary, Ph.D. thesis, Hebrew
 826 University of Jerusalem, Geological Survey of Israel Report No. GSI/24/98,
 827 Jerusalem, 231 pp. (in Hebrew, English abstract), 1998.
- 828 Avni, Y., and Zilberman, E.: Landscape evolution triggered by neotectonics in the Sede
 829 Zin region, central Negev, Israel, Israel J. Earth. Sci., 55, 189–208, 2007.
- 830 Bartov, Y., Agnon, A., Enzel, Y., and Stein, M.: Late Quaternary faulting and subsidence
 831 in the central Dead Sea basin, Israel, Israel J. Earth Sci., 55, 17–32, 2006.
- 832 Ben-Avraham, Z.: Structural framework of the Gulf of Elat (Aqaba), Northern Red Sea,
 833 J. Geophys. Res., 90(B1), 703–726, 1985.
- 834 Ben-Avraham, Z., and Schubert, G.: Deep "drop down" basin in the southern Dead Sea,
 835 Earth Planet. Sc. Lett., 251, 254–263, 2006.
- 836 Buchbinder, B., and Sneh, A.: Marine sandstones and terrestrial conglomerates and
 837 mudstones of Neogene – Pleistocene age in the Modi'im area: a re-evaluation,
 838 Geological Survey of Israel Current Research, 1983–84, 65–69. 1984.
- 839 Calvo, R.: Stratigraphy and petrology of the Hazeva Formation in the Arava and the
 840 Negev: Implications for the development of sedimentary basins and the
 841 morphotectonics of the Dead Sea Rift Valley, Ph.D. thesis, Hebrew University of
 842 Jerusalem, Geological Survey of Israel Report No. GSI/22/02, Jerusalem, 264 pp.
 843 (in Hebrew, English abstract), 2002.
- 844 Calvo, R., Bartov, Y., Avni, Y., Garfunkel, Z., and Frislander, U.: Geological field trip to
 845 the Karkom graben: The Hazeva Fm. and its relation to the structure, Annual
 846 Meeting Field Trips Guidebook, Israel Geological Society, pp. 47–62 (in Hebrew),
 847 1998.
- 848 Enzel, Y., Saliv, G., and Kaplan, M.: The tectonic deformation along the Zin Lineament,
 849 Nuclear Power Plant - Shivta Site: preliminary safety analysis Report. Appendix



- 850 2.5E: Late Cenozoic Geology in the Site area. Israel Electric Corporation Ltd.,
851 1988.
- 852 Enzel, Y., Kadan, G., and Eyal, Y.: Holocene earthquakes inferred from a Fan-Delta
853 sequence in The Dead Sea Graben, *Quaternary Res.*, 53, 34–48, 2000.
- 854 Eppelbaum, L., Ben-Avraham, Z., and Katz, Y.: Structure of the Sea of Galilee and
855 Kinarot Valley derived from combined geological-geophysical analysis, *First*
856 *Break*, 25(1), 21–28, 2007.
- 857 Eyal, Y., Kaufman, A., and Bar-Matthews, M.: Use of $^{230}\text{Th}/\text{U}$ ages of striated Carnotites
858 for dating fault displacements. *Geology*, 20, 829–832, 1992.
- 859 Farr, T. G., et al.: The Shuttle Radar Topography Mission, *Rev. Geophys.*, 45, RG2004,
860 <https://doi:10.1029/2005RG000183>, 2007.
- 861 Ferry, M., Meghraoui, M., Abou Karaki, N., Al-Taj, M., Amoush, H., Al-Dhaisat, S., and
862 Barjous, M.: A 48-kyr-long slip rate history for the Jordan Valley segment of the
863 Dead Sea Fault, *Earth Planet. Sc. Lett.*, 260, 394–406, 2007.
- 864 Garfunkel, Z.: Lateral motion and deformation along the Dead Sea transform, in: *Dead*
865 *Sea Transform Fault System: Reviews*, edited by: Garfunkel, Z., Ben-Avraham, Z.,
866 and Kagan, E. J., Springer, Dordrecht, the Netherlands, 109–150, 2014.
- 867 Ginat, H.: Paleogeography and the landscape evolution of the Nahal Hiyyon and Nahal
868 Zihor basins, Ph.D. thesis, Hebrew University of Jerusalem, Geological Survey of
869 Israel Report No. GSI/19/97, Jerusalem, 206 pp. (in Hebrew, English abstract),
870 1997.
- 871 Hartman, G., Niemi, T. M., Tibor, G., Ben-Avraham, Z., Al-Zoubi, A., Makovsky, Y.,
872 Akawwi, E., Abueladas, A.-R., and Al-Ruzouq, R.: Quaternary tectonic evolution
873 of the Northern Gulf of Elat/Aqaba along the Dead Sea Transform, *J. Geophys.*
874 *Res.: Solid Earth*, 119, 9183–9205, doi:10.1002/2013JB010879, 2014.
- 875 Hurwitz, S., Garfunkel, Z., Ben-Gai, Y., Reznikov, M., Rotstein, Y., and Gvirtzman, H.:
876 The tectonic framework of a complex pull-apart basin: seismic reflection



- 877 observations in the Sea of Galilee, Dead Sea transform. *Tectonophysics*, 359(3–4),
 878 289–306, 2002.
- 879 IEC and WLA (Israel Electric Corporation and William Lettis & Associates, Inc.):
 880 Shivta-Rogem Site Report. Israel Electric Corporation, Ltd., 2002.
- 881 Kafri, U., and Ecker, A.: Neogene and Quaternary subsurface geology and hydrogeology
 882 of the Zevulun plain, Geological Survey of Israel Bulletin No. 37, Jerusalem, 13
 883 pp., 1964.
- 884 Katz, O., Amit, R., Yagoda-Biran, G., Hatzor, Y. H., Porat, N., and Medvedev, B.:
 885 Quaternary earthquakes and landslides in the Sea of Galilee area, the Dead Sea
 886 Transform: paleoseismic analysis and implication to the current hazard, *Israel J.*
 887 *Earth. Sci.*, 58, 275–294, 2009.
- 888 Le Béon, M., Klinger, Y., Mériaux, A.-S., Al-Qaryouti, M., Finkel, R. C., Mayyas, O.,
 889 and Tapponnier, P.: Quaternary morphotectonic mapping of the Wadi Araba and
 890 implications for the tectonic activity of the southern Dead Sea fault. *Tectonics*, 31,
 891 TC5003, doi:10.1029/2012TC003112, 2012.
- 892 Marco, S., Hartal, M., Hazan, N., Lev, L. and Stein, M.: Archaeology, history and
 893 Geology of the A.D. 749 earthquake, Dead Sea transform, *Geology*, 31, 665– 668,
 894 2003.
- 895 Mitchell, S. G., Matmon, A., Bierman, P. R., Enzel, Y., Caffee, M., and Rizzo, D.:
 896 Displacement history of a limestone normal fault scarp, northern Israel, from
 897 cosmogenic ^{36}Cl , *J. Geophys. Res.*, 106(B3), 4247–4264, 2001.
- 898 Reznikov, M., Ben-Avraham, Z., Garfunkel, Z., Gvirtzman, H., and Rotstein, Y.:
 899 Structural and stratigraphic framework of Lake Kinneret, *Israel J. Earth. Sci.*, 53,
 900 131–149, 2004.
- 905 Sagy, A., and Nahmias, Y.: Characterizing active faulting zone, in: *Infrastructure*
 906 *instability along the Dead Sea: Final Report: 2008–2010*, edited by: Baer, G.,
 907 Geological Survey of Israel Report No. GSI/02/2011, Jerusalem, 7–17 (in Hebrew),
 908 2011.



- 909 Sagy, Y., and Gvirtzman, Z.: Subsurface mapping of the Zevulun valley, The
 910 Geophysical Institute of Israel Report 648/454/09, Lod, 21 pp. (in Hebrew), 2009.
- 911 Schattner, U., and Ben-Avraham, Z.: Transform margin of the northern Levant, eastern
 912 Mediterranean: From formation to reactivation, *Tectonics*, 26, TC5020,
 913 doi:10.1029/2007TC002112, 2007.
- 914 Schattner, U., and Weinberger, R.: A mid-Pleistocene deformation transition in the Hula
 915 basin, northern Israel: Implications for the tectonic evolution of the Dead Sea Fault,
 916 *Geochem. Geophys. Geosyst.*, 9(7), Q07009, doi: 10.1029/2007GC001937, 2008.
- 917 Sneh, A., and Weinberger, R.: Major geological structures of Israel and Environs,
 918 Geological Survey of Israel, Jerusalem, 2014.
- 919 Weinberger, R., Gross, M. R., and Sneh, A.: Evolving deformation along a transform
 920 plate boundary: Example from the Dead Sea Fault in northern Israel, *Tectonics*, 28,
 921 TC5005, doi:10.1029/2008TC002316, 2009.
- 922 Wieler, N., Avni, A., Ginat, H., and Rosensaft, M.: Quaternary map of the Eilat region on
 923 a scale of 10:000 with explanatory notes, Geological Survey of Israel Report No.
 924 GSI/37/2016, Jerusalem, 15 pp. (in Hebrew, English abstract), 2017.
- 925 Zilberman, E.: The geology of the central Sinai-Negev shear zone, central Negev. Part C:
 926 The Paran Lineament, Geological Survey of Israel Report No. GSI/38/85,
 927 Jerusalem, 53 pp., 1985.
- 928 Zilberman, E., Baer, G., Avni, Y., and Feigin, D.: Pliocene fluvial systems and tectonics
 929 in the central Negev, southern Israel, *Israel J. Earth. Sci.*, 45, 113–126, 1996.
- 930 Zilberman, E., Greenbaum, N., Nahmias, Y., Porat, N., and Ashqar, L.: Middle
 931 Pleistocene to Holocene tectonic activity along the Carmel Fault - preliminary
 932 results of a paleoseismic study, Geological Survey of Israel Report No.
 933 GSI/02/2007, Jerusalem, 35 pp., 2006.
- 934 Zilberman, E., Greenbaum, N., Nahmias, Y., Porat, N., and Ashkar, L.: Late Pleistocene
 935 to Holocene tectonic activity along the Nesher fault, Mount Carmel, Israel, *Israel J.*
 936 *Earth. Sci.*, 57, 87–100, 2008.



- 937 Zilberman, E., Nahmias, Y., Gvirtzman, Z., and Porat, N.: Evidence for late Pleistocene
938 and Holocene tectonic activity along the Bet Qeshet fault system in the Lower
939 Galilee, Geological Survey of Israel Report No. GSI/06/2009, Jerusalem, 22 pp. (in
940 Hebrew, English abstract), 2009.
- 941 Zilberman, E., Ron, H., Sa'ar, R.: Evaluating the potential seismic hazards of the Ahihud
942 Ridge fault system by paleomagnetic and morphological analyses of calcretes,
943 Geological Survey of Israel Report No. GSI/15/2011, Jerusalem, 30 pp., 2011.
- 944
- 945